sustainability

MDPI

Article

Fatala River Basin (Republic of Guinea, Africa): Analysis of Current State, Air Pollution, and Anthropogenic Impact Using Geoinformatics Methods and Remote Sensing Data

Vladimir Tabunschik *, Roman Gorbunov, Nikolai Bratanov, Tatiana Gorbunova, Natalia Mirzoeva and Veronika Voytsekhovskaya

A.O. Kovalevsky Institute of Biology of the Southern Seas of RAS, 299011 Sevastopol, Russia; karadag_station@mail.ru (R.G.); bratanov@ibss-ras.ru (N.B.); gorbunovatyu@ibss-ras.ru (T.G.); natmirz@mail.ru (N.M.); voitsekh@ibss-ras.ru (V.V.)

* Correspondence: tabunshchyk@ibss-ras.ru

Abstract: This study conducts an in-depth analysis of anthropogenic transformation and air pollution within the confines of the Fatala River Basin situated in the Republic of Guinea, Africa. The foundation of this investigation relies upon interdisciplinary geoinformatics methodologies and data acquired through remote sensing, specifically drawing from Sentinel-5P and Sentinel-2 satellite datasets. The primary objectives encompass scrutinizing the extant ecological conditions characterizing the Fatala River Basin and assessing the anthropogenic influences within its geographic expanse. The utilization of remote sensing data, as facilitated by the Sentinel-5P satellite, emerges as a potent instrument for meticulously monitoring environmental transformations. A comprehensive analysis of the designated area, conducted through remote sensing methodologies, is employed to ascertain the concentrations of various atmospheric constituents, including nitrogen dioxide, sulfur dioxide, formaldehyde, methane, ozone, and carbon monoxide. The findings gleaned from this inquiry reveal that, notwithstanding the dynamic growth of the extractive industry centered around the world's preeminent bauxite province, the Fouta Djallon–Mandingo, the anthropogenic transformation of the Fatala River Basin exerts a comparatively minor influence on air quality. Statistical assessments, including correlation analysis, conducted between computed parameters delineating anthropogenic alterations within the Fatala River Basin, and a comprehensive atmospheric pollution index elucidate a lack of a significant nexus. It has been determined that air pollution within the Fatala River Basin is notably influenced by topographical features and the transport of contaminants from adjacent river basins. Consequently, this article makes a substantial contribution to our comprehension of the contemporary ecological state of the Fatala River Basin in the Republic of Guinea. It also holds significant importance in elucidating the ecological challenges specific to the researched region.

Keywords: Fatala River Basin; Africa; Republic of Guinea; anthropogenic transformation; air pollution; Sentinel-5P

Citation: Tabunschik, V.; Gorbunov, R.; Bratanov, N.; Gorbunova, T.; Mirzoeva, N.; Voytsekhovskaya, V. Fatala River Basin (Republic of Guinea, Africa): Analysis of Current State, Air Pollution, and Anthropogenic Impact Using Geoinformatics Methods and Remote Sensing Data. *Sustainability* **2023**, *15*, 15798. https://doi.org/10.3390/su152215798

Academic Editors: Yiping Chen, Yan Zhao, Jifu Ma and Dong Chen

Received: 10 October 2023
Revised: 6 November 2023
Accepted: 7 November 2023
Published: 9 November 2023

1. Introduction

Since the 20th century, there has been a continuous and escalating adverse impact on natural landscapes across various regions worldwide [1–3]. The most pronounced anthropogenic influence has been evident in the reduction of forested areas, the destruction of natural habitats [4,5], mineral extraction activities [6,7], pollution of rivers and water bodies [8,9], urbanization expansion [10,11] (often unregulated in developing nations), and air pollution [12,13]. Concurrently, this trend has created additional conditions conducive to erosion [14,15], floods [16,17], landslides and avalanches [18,19], wildfires [20,21], and climate change [22,23] as a result of anthropogenic activities. These activities, in many instances, fail to consider the natural physical-geographical and historical nuances of regions and, regrettably, are frequently conducted without proper oversight.

In developed countries in Europe and North America, the crises that were prevalent in the latter half of the 20th century have, to some extent, been mitigated. These regions have established robust regulatory frameworks for environmental protection and the reduction of anthropogenic impacts [24,25]. Conversely, in developing nations, there is an observable pattern of relocating polluting industries from developed countries to their territories, leading to an exacerbation of environmental harm. In recent years, this issue has become highly pertinent for Africa, a continent rich in natural resources. These resources often necessitate exploration, with their extraction proving to be relatively cost-effective for transnational corporations [26]. Africa boasts substantial reserves of oil, gas, and both ferrous and non-ferrous metals. Notably, mining operations in Africa are frequently executed through open-pit methods, inflicting considerable damage on the surrounding natural environment. A primary driver of adverse ecological consequences is mineral extraction, including open-pit and semi-open-pit methodologies [27–29]. Despite relatively low population densities in many African regions, it is the expansion of the mining sector that has a considerable impact on environmental degradation.

The Republic of Guinea has emerged as a prominent player in the global mining industry [30–32]. Notably, approximately 90% of mining operations in the Republic of Guinea employ open-pit techniques for ore extraction, a practice known to inflict significant ecological damage [33]. While extensive research has scrutinized coastal water pollution in the Republic of Guinea and other Gulf of Guinea bordering nations [34,35], terrestrial pollution within the country, particularly in the context of mining activities, has been subject to limited scholarly inquiry [36,37].

At the same time, the Republic of Guinea is a global leader in industrial bauxite reserves. There is a significant amount of research dedicated to assessing the impact of bauxite mining activity in the Republic of Guinea [38–40]. Sanoh et al. [41] assert that Guinea's bauxite reserves constitute approximately 24% of the world's total. Furthermore, as underscored in academic sources [42,43], Guinean bauxite boasts exceptionally high quality. This extractive industry predominantly centers its operations within the western and northwestern regions of the Republic of Guinea. Diallo et al. [37] underscore the adverse environmental impact of bauxite mining in these specific regions, primarily attributed to the destructive nature of open-pit mining, often entailing the obliteration of natural vegetation. This practice ranks as one of the most environmentally devastating forms of mineral extraction, particularly within tropical forests [37]. It is noteworthy that comprehensive research on environmental pollution within the water bodies and landscapes of the Republic of Guinea remains relatively insufficient [37,44,45]. J. Knierzinger [46] provides an illustrative case wherein the surge in bauxite mining has correlated with the expansion of human settlements and their populations. Nonetheless, scant attention has been devoted to scrutinizing the adverse facets of bauxite extraction by transnational corporations.

In a parallel academic discourse, Ji et al. [1] draw our attention to the pivotal role played by anthropogenic disruptions in landscape transformations. These disruptions have precipitated a slew of adverse consequences for rivers and their respective basins. The river basins of the Republic of Guinea do not elude the repercussions of this anthropogenic influence, with the Fatala River Basin serving as a salient exemplar of such impacts.

The aim of this study is to investigate the anthropogenic transformation of the Fatala River Basin (Republic of Guinea, Africa). To achieve this goal, the following objectives must be addressed: (1) Conduct geoinformation modeling and delineate the boundaries of the Fatala River Basin; (2) Calculate values of indicators characterizing anthropogenic transformation within the Fatala River Basin (anthropogenic transformation coefficient, land anthropogenic disturbance index, urbanization coefficient, degree of anthropogenic transformation, natural protection coefficient) and demonstrate their spatial variability; (3) Identify the concentrations of nitrogen dioxide, sulfur dioxide, formaldehyde, methane, carbon oxide, and ozone in the air within the Fatala River Basin; (4) Determine the extent of the impact of anthropogenic transformation on air pollution within the territory of

the Fatala River Basin; (5) Identify the primary sources of pollution and demonstrate the spatial-temporal variability of pollutant fields.

Section 1 presents the history of research on the subject and the research issues raised by the authors. Section 2 provides a description of the study area, the Fatala River Basin, and offers a detailed explanation of the research methodology. Section 3 presents the research results and describes the spatial differentiation of indicators of anthropogenic transformation and air pollution within the Fatala River Basin. Section 4 conducts an analysis of the obtained data, compares them with similar data from other regions of the world, outlines the limitations of the study, and discusses prospects for further research. Finally, Section 5 presents the concluding remarks and findings of the study.

2. Materials and Methods

2.1. Study Area

The study area encompasses the Fatala River Basin, with a total land area of 692 km^2. The Fatala River Basin is located at 12°76′–14°11′ W, 10°06′–11°05′ N. This area is situated in Western Africa, falling within the boundaries of the Republic of Guinea, as depicted in Figure 1.

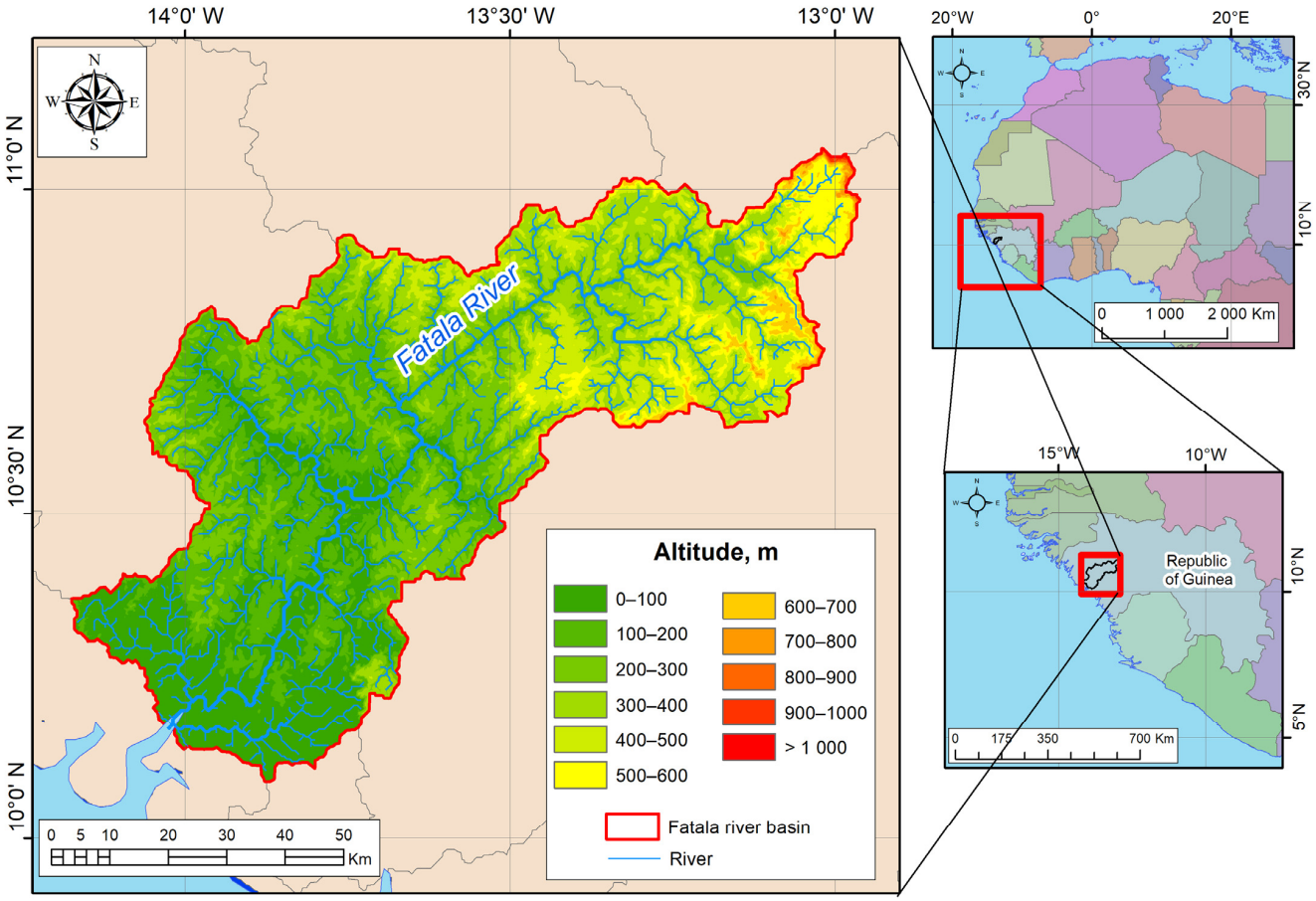

Figure 1. Geographic Position of the Fatala River Basin.

The riverbed of the Fatala River spans two administrative regions, Boke and Kindia. During the wet season, the Fatala River assumes the role of a significant transportation artery, directly connecting to the Atlantic Ocean Basin. This accessibility facilitates the advancement of mineral resource extraction activities within the Futa-Jalon Plateau.

The study area is located upon the ancient African platform of the Precambrian folded basement. Tectonically, it is ensconced between two prominent tectonic structures. The southern boundary adjoins the Sierra Leone Shield, distinguished by Kibaran-age granitic

intrusions that penetrate the Precambrian folded basement. Meanwhile, the northern limit is demarcated by the Senegalese syncline. The terrain is characterized by a platform covering, predominantly composed of sandstones dating back to the Paleozoic era, Ordovician and Devonian formations, graptolite shales, as well as aleurolites and argillites [47]. Along the Atlantic Ocean shoreline, a strip of alluvial and marine deposits is evident.

The research area is situated within the equatorial climatic zone, typified by a tropical monsoon climate on the western coast. Two distinct seasons predominate—a humid summer and a dry winter. The annual count of rainy days escalates to approximately 170. During the wet season, average precipitation levels may surge to 3700 mm. Conversely, the dry season is marked by exceptionally scanty rainfall, with an average of merely 19 mm. The yearly mean air temperature stands at 26 °C, maintaining an amplitude of 5–6 °C throughout the entire year.

The Fatala River Basin finds its location within the system of stepped high plateaus characteristic of the Futa-Jalon Plateau [48]. The initial plateau steps are situated in close proximity to the coastal plains of the Atlantic Ocean. Progressing eastward, there is a gradual elevation in terrain, culminating at 150–200 m. The central part of the plateau reaches an average elevation of 800–1000 m. A distinctive feature of this territory is its markedly dissected relief, a consequence of the erosional processes driven by river dynamics, ultimately leading to denudation and the formation of temporary watercourses during the wet season.

The river basin under study is situated within the Paleotropical floristic region and encompasses several distinct vegetation types. Its source is located in a transitional zone from humid tropical forests to intermittently moist Kazamans-type forests. Among the dominant tree species in this area are *Parinari excelsa*, *Erythrophleum guineense*, *Detarium senegalense*, and *Afzelia africana*. Moving towards the central part of the basin, the landscape transitions into a zone characterized by deciduous and evergreen, intermittently moist tropical forests. Notable woody vegetation includes *Pandanus*, *Ficus*, and *Hymenocardia acida*. Moreover, substantial expanses of herbaceous vegetation, predominantly comprising *Pennisetum purpureum* and *Loudetia arundinacea*, can be observed. Finally, at the river's estuary along the Atlantic Ocean coastline, one can find thriving West African mangroves, dominated by *Rhizophora*, *Laguncularia racemosa*, and *Conocarpus erectus* [49–51].

The source of the Fatala River is situated in the western region of the Republic of Guinea, specifically within the Fréa area of the Futa-Jalon Plateau. Spanning a total length of 205 km, the river eventually discharges into the Rio Pongo before finally reaching the Atlantic Ocean [52]. The territory of the Republic of Guinea serves as the watershed between two major river systems. The primary source of water for the Fatala River is rainfall, with a significant portion occurring during the wet season, which coincides with the summer months. As a result, high water levels are prevalent during the rainy season [52].

The study area encompasses three principal soil types commonly found in African landscapes. In the northeastern part of the Fatala River Basin, lithic leptosols prevail, characterized by shallow soil layers with a substantial presence of gravel material and exposed bedrock. Taxonomically, the majority of these soils fall under the classification of entisols [53].

Moving towards the central part of the basin, there is a transition to red ferrallitic soils [53]. These soils are characterized by leaching processes leading to nearly complete mineral weathering within the soil composition. Consequently, stable products like aluminum oxides, iron oxides, and kaolinite come to dominate the chemical composition of the ferralsols, imparting them with distinct red and yellow colors. Calcium and magnesium levels in these soils are exceedingly low. A significant portion of the study area undergoes the active formation of lateritic profiles, constituting the largest bauxite-bearing province in Fouta Djallon–Mandingo, accounting for 50% of all tropical bauxite deposits [54]. According to data provided by R. Manheim, laterite profiles can extend to depths exceeding 700 cm [55].

Coastal areas within the study region are characterized by thionic fluvisols, which exhibit sediment stratification resulting from water deposition [53]. The presence of an acidic horizon with a rich sulfur content can be traced in the soils. Soil characteristics for each layer are contingent upon factors such as the duration of soil formation and the intervals between or after flooding events. These factors contribute to soil variations, ranging from gravelly-sandy textures to fine-grained soils intermixed with organic remnants.

2.2. Research Methodology

The comprehensive methodology for assessing anthropogenic transformation and air pollution within the Fatala River Basin is delineated in Figure 2.

The demarcation of the Fatala River Basin was executed employing a digital elevation model sourced from Copernicus [56]. This process was facilitated using the ArcGIS 10.8 software suite (ESRI, Redlands, CA, USA), adhering to the established methodologies detailed in numerous scholarly works [57–59]. The maps utilized in this study have been constructed within the "World Geodetic System 1984" (WGS 84, EPSG: 4326) projection. For area measurements, we also utilized shapefiles delineating land-use types and the boundaries of the Fatala River Basin, presented in the UTM 28N projection (EPSG: 32628).

Land-use classifications were derived from the analysis of Sentinel-2 satellite imagery [60] characterized by a spatial resolution of 10 m. Supervised classification was carried out in the study. The outcome of this analysis yielded a comprehensive understanding of the primary land-use categories within the confines of the Fatala River Basin.

To quantify anthropogenic transformation within the Fatala River Basin, ArcGIS software was employed, encompassing both the entirety of the basin and 1×1 km grid cells that collectively covered the basin's expanse. The basin's territory was discretized into 1×1 km grid cells through the utilization of ArcGIS 10.8 (ESRI, Redlands, CA, USA). For both the overall Fatala River Basin and each individual grid cell, land areas allocated to various land-use categories were systematically quantified. Based on these land area assessments, a suite of indices characterizing anthropogenic transformation (including the coefficient of anthropogenic transformation, the index of anthropogenic land disturbance, urbanization coefficient, the degree of anthropogenic transformation, and coefficient of natural protection) [61] were meticulously computed. Subsequently, maps of the considered indices are constructed.

Air quality data, encompassing concentrations of ozone, methane, nitrogen dioxide, sulfur dioxide, carbon monoxide, and formaldehyde, were acquired leveraging the Sentinel-5P satellite and the computational resources of the Google Earth Engine platform [62,63]. For the evaluation of pollutant concentrations, the "Sentinel-5P L3" collection was harnessed (e.g., for carbon monoxide—ee.ImageCollection ("COPERNICUS/S5P/OFFL/L3_CO")). Following data acquisition, a series of data filtration techniques and data processing procedures (including spatial cropping to the boundaries of the study area) were systematically applied. The data were filtered by time periods (annual averages). This was followed by a comprehensive analysis of the resulting raster datasets. Subsequently, the procured data were securely stored utilizing Google Drive. The presentation of geographical maps was executed using the ArcGIS software package. The calculation of the complex index of atmospheric pollution (CIAP) was underpinned by reference values established within the confines of the protected natural domain, specifically, the Moyen-Bafing National Park, the precise delineation of which was acquired from [64].

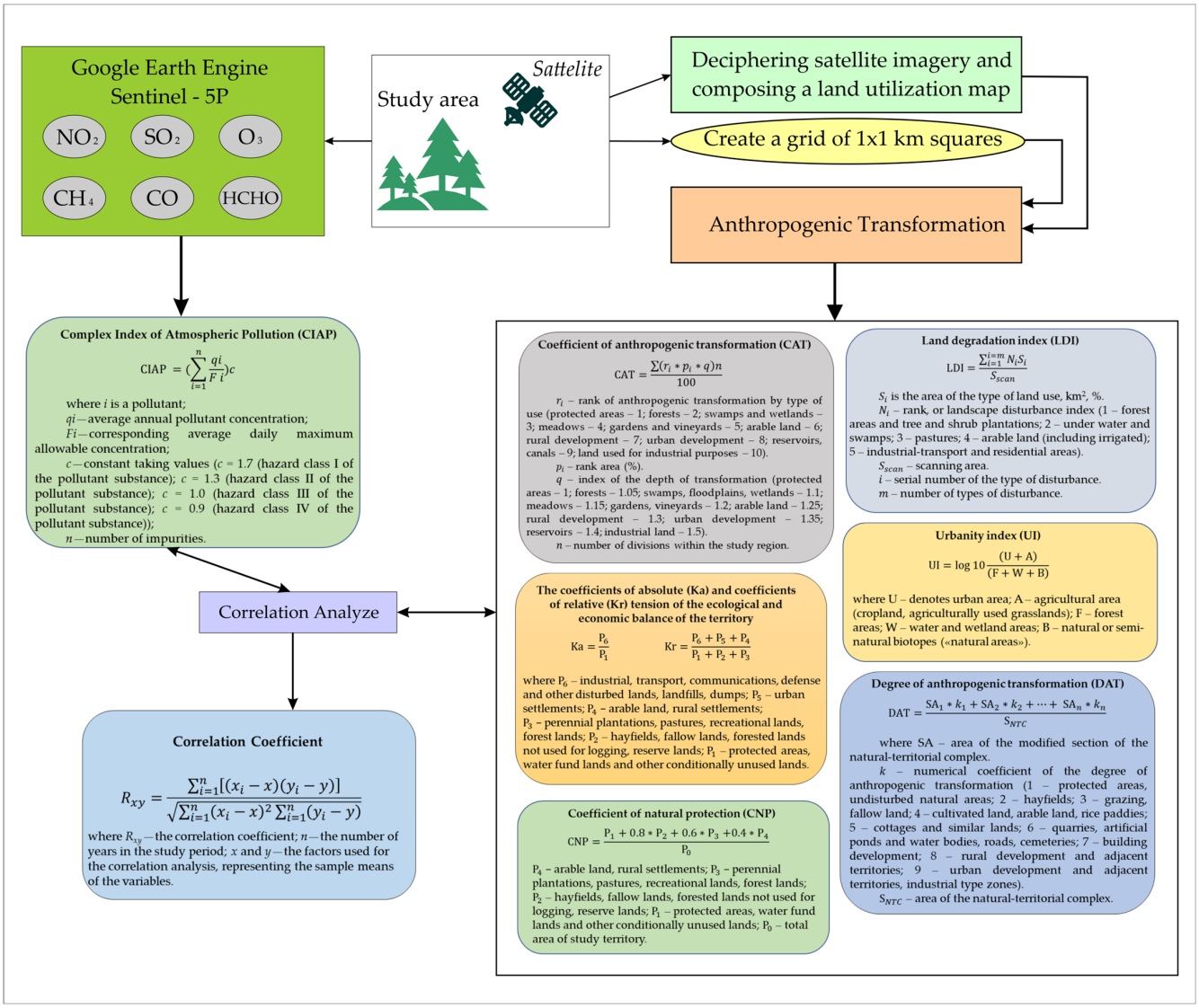

Figure 2. Methodology for investigating anthropogenic transformation and air pollution within the Fatala River Basin (compiled on the basis of [61,63] with additions from the authors).

3. Results

3.1. Anthropogenic Transformation of the Fatala River Basin

Figure 3 presents a comprehensive overview of various indices designed to characterize the degree of anthropogenic transformation within the Fatala River Basin.

As depicted in Figure 3, the overall extent of anthropogenic transformation across the Fatala River Basin predominantly falls within the low to moderate range. While certain localized regions within the study area exhibit elevated values across various transformation indices, these occurrences are often associated with specific local factors and the historical evolution of the Fatala River Basin. Notably, the most heavily transformed areas tend to be those adjacent to major population centers such as Boffa, Telimele, and Fria, as well as localized zones characterized by intensive mining and industrial activities. Table 1 provides a summary of the minimum, maximum, and average values for the examined anthropogenic transformation indicators within the Fatala River Basin.

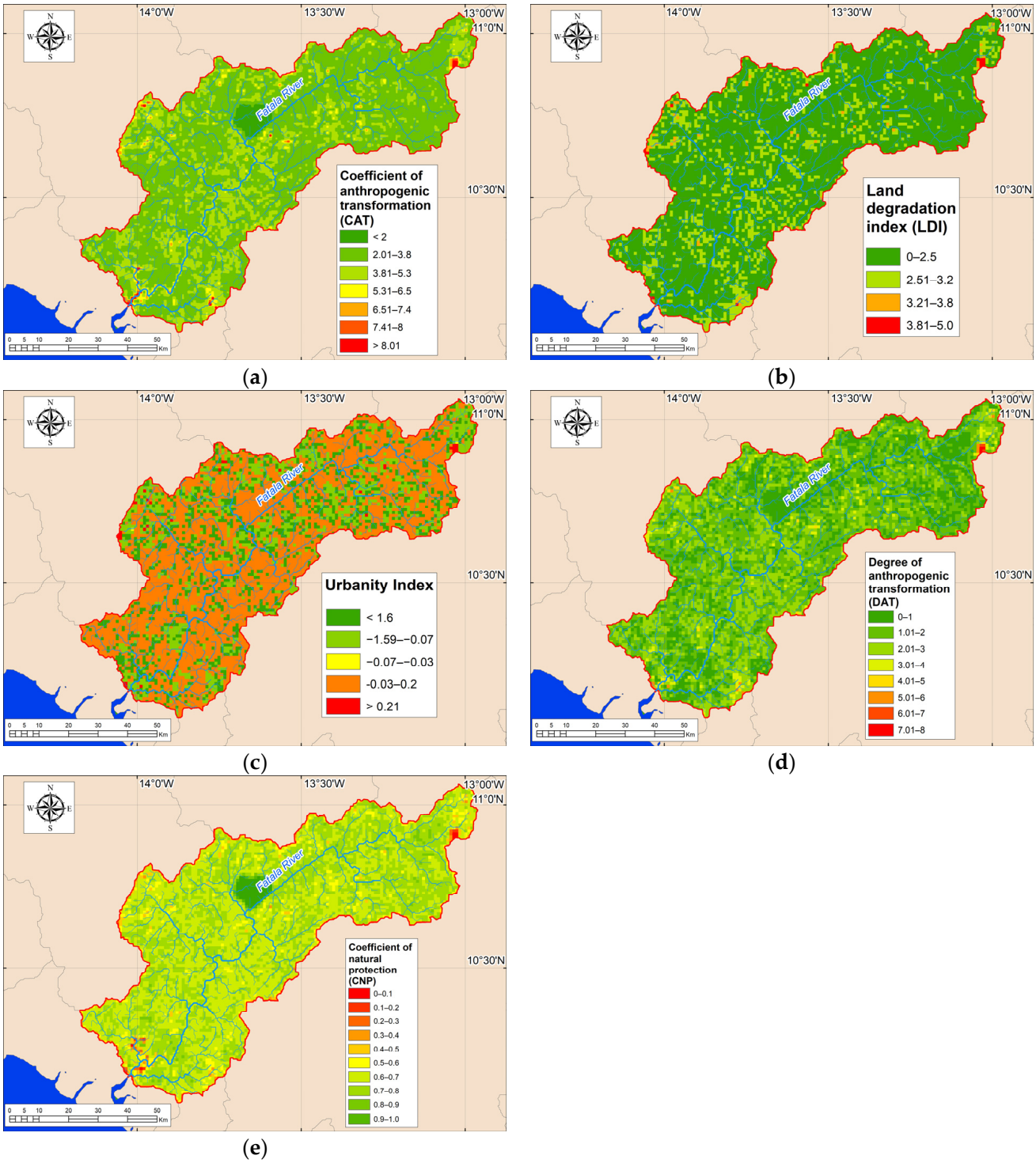

Figure 3. Anthropogenic transformation of the Fatala River Basin: (**a**) coefficient of anthropogenic transformation (CAT); (**b**) land degradation index (LDI); (**c**) urbanity index (UI); (**d**) degree of anthropogenic transformation (DAT); (**e**) coefficient of natural protection (CNP).

Table 1 reveals that, although there are notable instances of high maximum values in the examined anthropogenic transformation indicators, the average values for the entire Fatala River Basin consistently remain relatively low. These averages depict the basin as moderately to weakly transformed on the whole. Table 2 presents the distribution of these transformation indicators across distinct altitude ranges within the Fatala River Basin for further analysis.

Table 1. Minimum, maximum, and average values of various anthropogenic transformation indicators in the Fatala River Basin.

Indicators	Values		
	Minimum	**Maximum**	**Average**
Coefficient of anthropogenic transformation	1.00	12.60	3.51
Land degradation index	0.00	5.00	2.01
Urbanity index	−6.00	2.95	−0.67
Degree of anthropogenic transformation	0.00	8.00	1.61
Coefficients of absolute tension of the ecological and economic balance of the territory	0.00	0.11	-
Coefficients of relative tension of the ecological and economic balance of the territory	0.00	893.13	0.25
Coefficient of natural protection	0.00	1.00	0.68

Table 2. Distribution of values for various anthropogenic transformation indicators within the Fatala River Basin across absolute altitude ranges.

Altitude, m	Coefficient of Anthropogenic Transformation	Land Degradation Index	Urbanity Index	Degree of Anthropogenic Transformation	Coefficient of Natural Protection
0–100	3.80	2.12	−0.69	1.83	0.66
100–200	3.49	2.05	−0.62	1.62	0.69
200–300	3.37	1.93	−0.61	1.54	0.70
300–400	3.29	1.89	−0.71	1.40	0.70
400–500	3.52	2.04	−0.76	1.57	0.67
500–600	3.59	2.09	−0.71	1.75	0.66
600–700	3.21	1.87	−0.54	1.32	0.66
700–800	2.89	1.60	−0.87	0.93	0.63
800–900	3.13	1.76	−0.92	1.22	0.58
900–1000	3.05	1.70	−0.48	1.12	0.65
1000–1025	2.33	1.18	−2.65	0.28	0.13

The coefficients indicating anthropogenic transformation exhibit a range from 2.33 to 3.80. A noteworthy observation is that these coefficients decrease as elevation increases, specifically within the altitude interval of 0 to 400 m. This trend underscores that human impact on the environment is most pronounced in the lower regions of the Fatala River Basin, where elevations are below 400 m. Within the altitude range spanning 300 to 600 m, the coefficient of anthropogenic transformation experiences a marginal increase before declining once more. This pattern is mirrored in all other computed metrics.

As evidenced by Table 2, a consistent trend reveals a reduction in anthropogenic transformation across the Fatala River Basin as absolute elevations ascend and as one proceeds upstream. This phenomenon is chiefly linked to the historical development of the river basin and the heightened relief complexity observed in the middle and upper reaches of the basin.

3.2. Atmospheric Pollution in the Fatala River Basin

Table 3 presents comprehensive data encompassing the minimum, maximum, and average concentrations of atmospheric pollutants over the period from 2019 to 2022. Figures A1–A6 (Appendix A) show the distribution of fields of various pollutants within the Fatala River Basin.

The spatial-temporal distribution patterns of various substances, as depicted in Figures A1–A6 (Appendix A), reveal intricate dynamics. Broadly speaking, there exists a discernible trend associated with decreasing concentrations of chemical substances in the atmosphere towards the upper reaches of the Fatala River Basin.

Table 3. Annual minimum, maximum, and average concentrations of atmospheric pollutants within the Fatala River Basin.

Pollutants/Year	CH_4	CO	HCHO	NO_2	SO_2	O_3
Annual Minimum Concentrations						
2019	1823.4	0.039	0.000176	0.000017	0	0.117
2020	1848.2	0.038	0.000173	0.000015	0	0.120
2021	1839.7	0.039	0.000182	0.000015	0	0.120
2022	1848.9	0.036	0.000170	0.000016	0	0.121
Annual Maximum Concentrations						
2019	1887.9	0.043	0.000240	0.000028	0.000101	0.119
2020	1893.7	0.044	0.000249	0.000023	0.000139	0.121
2021	1914.7	0.044	0.000252	0.000026	0.000149	0.121
2022	1911.3	0.043	0.000250	0.000026	0.000121	0.122
Annual Average Concentrations						
2019	1860.5	0.041	0.000210	0.000021	0.000018	0.118
2020	1872.8	0.042	0.000214	0.000018	0.000044	0.121
2021	1883.3	0.042	0.000216	0.000020	0.000058	0.120
2022	1896.9	0.040	0.000210	0.000021	0.000044	0.122

To establish a comparative reference for pollution levels, the Moyen-Bafing National Park, an ecologically protected area adjacent to the Fatala River Basin, was chosen as a representative backdrop. Table 4 presents the mean background pollutants values from 2019 to 2022 within the Moyen-Bafing National Park.

Table 4. Background concentrations of atmospheric pollutants within protected natural areas (reference source—Moyen-Bafing National Park).

Pollutants	Sentinel-5P Background Value in Protected Natural Areas	Hazard Class
CH_4	1877.77	4
CO	0.0372	4
HCHO	0.000184	1
NO_2	0.000018	2
SO_2	0.000022	3
O_3	0.1200	1

The mean CIAP within the Fatala River Basin for the period 2019–2022 stands at 7.35. Generally, the CIAP values range from 5.34 to 9.52 (see Figure 4).

Lower CIAP values are characteristic of the upper basin of the Fatala River, while higher values are observed near the city of Fria. It is noteworthy that Fria, although geographically situated outside the Fatala River Basin, exerts the greatest influence on the study region.

3.3. The Relationship between CIAP and Various Anthropogenic Transformation Coefficients in the Fatala River Basin

To assess the influence of anthropogenic activities on air quality within the Fatala River Basin, we computed correlation coefficients between the CIAP and diverse coefficients that characterize anthropogenic transformation, such as the anthropogenic transformation coefficient, land degradation index, urbanization index, degree of anthropogenic transformation, and coefficient of natural protection. Figure 5 illustrates the spatial distribution of these correlation coefficients within the Fatala River Basin.

Figure 5 shows a predominantly weak correlation between indicators characterizing atmospheric pollution and anthropogenic transformation across the Fatala River Basin. Considering the entire basin, the correlation coefficients between CIAP and CAT values stand at −0.03. Correspondingly, for CIAP values against the LDI, the coefficient is −0.01. The UI exhibits a correlation of 0.02, while the DAT a coefficient of 0.01. Additionally,

CIAP values and CNP values show a correlation of 0.09. Consequently, anthropogenic transformation showcases minimal influence on atmospheric air pollution within the Fatala River Basin, substantiated by the very weak correlation coefficients. However, localized regions within the basin, indicated in Figure 5, display moderate to moderate-high correlation coefficients, though their impact remains constrained.

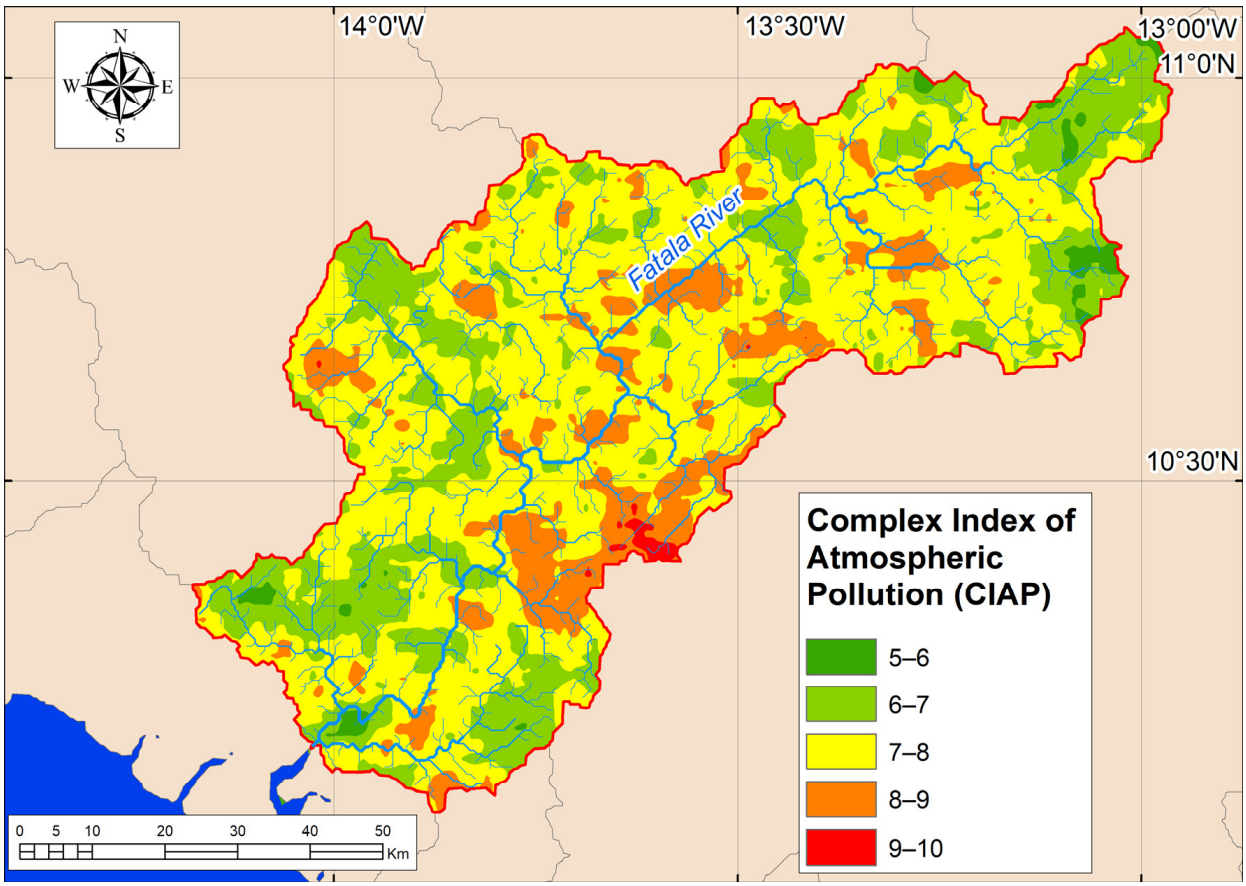

Figure 4. CIAP within the Fatala River Basin from 2019 to 2022.

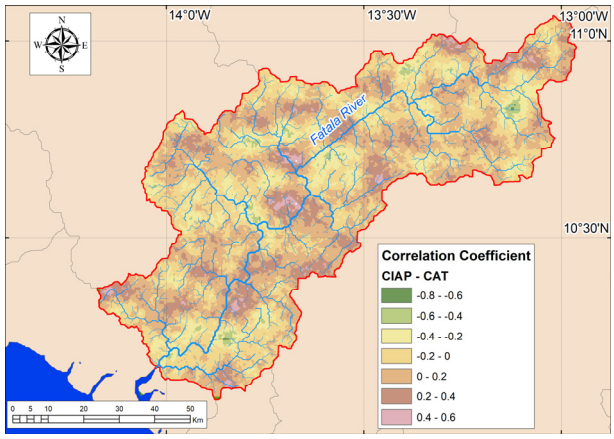

(**a**)

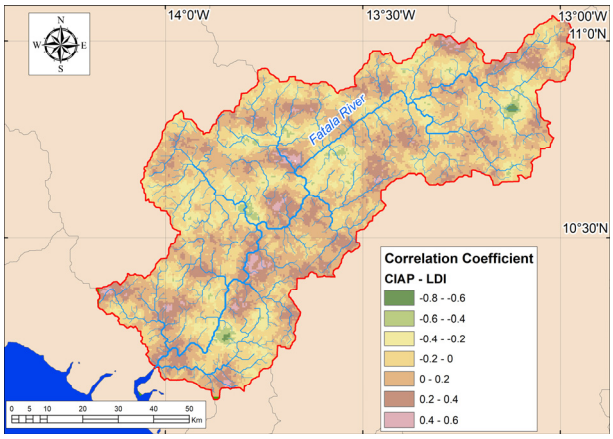

(**b**)

Figure 5. *Cont.*

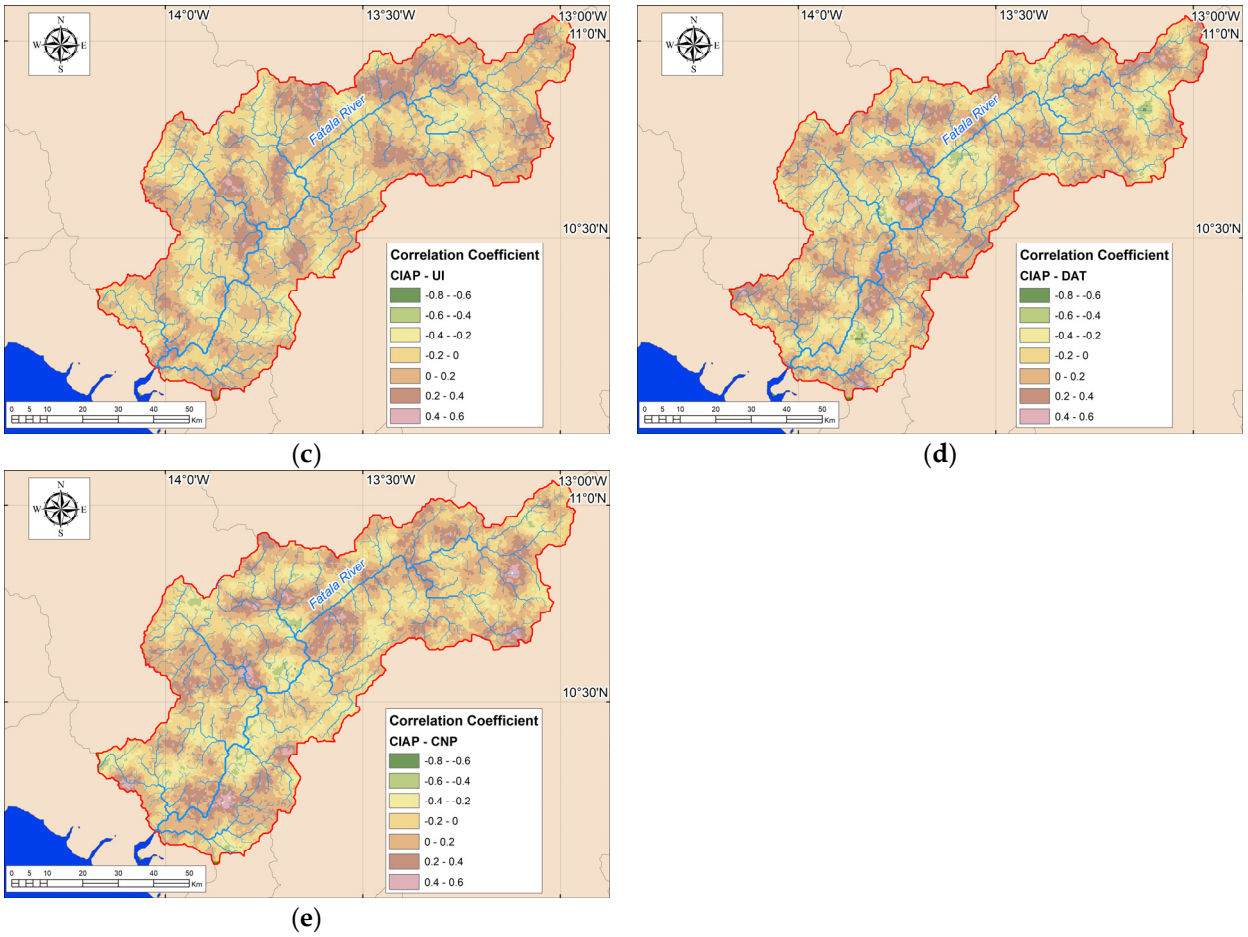

Figure 5. Spatial distribution of correlation coefficients in the Fatala River Basin between the CIAP and various anthropogenic transformation indicators: (**a**) coefficient of anthropogenic transformation (CAT); (**b**) land degradation index (LDI); (**c**) urbanity index (UI); (**d**) degree of anthropogenic transformation (DAT); (**e**) coefficient of natural protection (CNP).

3.4. Influence of Air Mass Transport on Air Pollution in the Fatala River Basin

To pinpoint the sources of air pollution within the Fatala River Basin, an exhaustive analysis of air pollutant distributions in regions adjacent to the Fatala River Basin was conducted. Figures A7–A12 (Appendix B) meticulously outline the dispersion patterns of key air pollutants, including nitrogen dioxide, sulfur dioxide, formaldehyde, methane, and carbon monoxide across the West African region.

As illustrated in Figure A10 (Appendix B), the spatial distribution of sulfur dioxide pollution is influenced by the atmospheric transport from Senegal and Gambia. Figures A7–A9 (Appendix B) indicate that the primary sources of nitrogen dioxide, formaldehyde, and carbon monoxide pollution are centered around the capital of the Republic of Guinea and neighboring countries, particularly Senegal. Due to the complex relief within the Republic of Guinea, characterized by extensive mountainous areas and plateaus, the distribution of pollutant concentrations exhibits significant variability across different altitudinal ranges (Tables A1–A4 (Appendix C)).

As evident from Tables A1–A4 (Appendix C), a consistent trend emerges where the concentrations of carbon monoxide, methane, and ozone decline with increasing absolute altitudes within the Fatala River Basin. Conversely, for formaldehyde, nitrogen dioxide, and sulfur dioxide, such a correlation with altitude is not apparent.

4. Discussion

Within the territory of the Fatala River Basin, the distribution of pollutants exhibits a complex pattern. The spatial-temporal distribution of pollution indicators is significantly influenced by the relief within the Fatala River Basin and its adjacent areas. Surprisingly, even within protected areas like the Counsignaki Classified Forest, which are expected to experience minimal anthropogenic influence (as depicted in Figure 3), significant pollution hotspots for various chemical substances are observed. This anomaly is particularly evident for formaldehyde, sulfur dioxide, carbon dioxide, and carbon monoxide. The comprehensive air pollution index (Figure 4) reveals substantial pollution levels within this protected area. The primary reason for this anomaly lies in the inclusion of the research area within the "tail" of an atmospheric pollution transport corridor, as visually depicted in Figures A7–A10 (Appendix B). This occurrence is closely tied to the barrier effect exerted by the Fouta Djallon Plateau, which disrupts traditional models of air mass movement along the western coasts during tropical monsoons. This situation leads to a scenario where the barrier effect not only affects precipitation patterns on the slope but also results in a significant accumulation of dust particles generated during open bauxite mining. The Fouta Djallon mountain system's barrier effect causes anthropogenically released elements to migrate towards the foothills and plateau bases, where they accumulate due to the lack of further transportation with air masses.

Figure 6 provides a visualization of the spatial variability in predominant annual wind directions across sixteen cardinal points, constructed based on data sourced from the ERA-5 reanalysis [65]. Figure 6 affords us a comprehensive perspective on the influence exerted by prevailing air masses and the terrain on the redistribution of pollutant flows. Over the course of the year, the transport of air masses predominantly originates from the Atlantic Ocean (Guinea Gulf) and extends inland into the African continent. Nevertheless, this transport encounters disruption due to local orographic factors in West Africa. Air masses are significantly redistributed owing to the barrier effect caused by the Fouta Djallon Plateau (which reaches elevations of up to 1538 m) in Guinea, the Loma Mountains (rising to elevations of up to 1950 m) in Sierra Leone, and the Leone-Liberian Massif (with elevations reaching up to 1948 m) in Liberia and Sierra Leone. These factors render the western and southwestern slopes of these orographic features particularly susceptible to pollutant impacts. The presence of orographic barriers compels air masses, predominantly characterized by westward trajectories over the Atlantic Ocean, to deviate towards the southwesterly and southerly directions, and they further propagate along river valleys. Notably, the movement of methane, formaldehyde, nitrogen dioxide, carbon monoxide, sulfur dioxide, and ozone is distinctly influenced by orographic barrier effects. Furthermore, the distribution of sulfur dioxide pollution is significantly influenced by the transport of air masses. Nevertheless, it is essential to note that the principal source of sulfur dioxide pollution resides in Dakar (Senegal), situated on the Cape Verde Peninsula, which protrudes into the Atlantic Ocean and is encompassed by the Ferlo Desert to the south—a region that adjoins the Fouta Djallon Plateau. Consequently, predominant winds in the vicinity of Dakar tend to blow in a northward and northwestward direction. As a result, sulfur dioxide pollution disperses over land in the south and southeast, as well as over the ocean to the south. This dispersion pattern, coupled with the southwestward transport of air masses in lower latitudes, contributes to the presence of pollutants in countries bordering the Gulf of Guinea, including the Fatala River Basin.

While one might anticipate that the major population centers located within the Fatala River Basin, such as Boffa (with an approximate population of 10,000) and Télimélé (housing approximately 16,000 residents), would exhibit the highest pollution levels, our analyses reveal a different pattern. For several pollutant indicators, particularly nitrogen dioxide, these urban areas and their adjacent regions emerge as the least polluted. This observation is primarily attributed to the fact that the primary local sources of pollution are situated along the middle reaches of the Fatala River, represented by localized mining enterprises that emit substantial quantities of pollutants into the atmosphere. Additionally, the influence of

seasonal air mass transport patterns and the barrier effects of the region's mountains and ridges play pivotal roles. These influences deviate markedly from the global and African patterns of pollution distribution, where the highest emissions are typically associated with major urban centers. An examination of Figures A7–A12 (Appendix B) offers insights into the distribution of pollutants in Western Africa and the region bordering the Fatala River Basin, highlighting the highest emissions in capital cities. This concentration of pollution is primarily linked to the historical development of the region and the concentration of industries in major cities, many of which serve as major port hubs.

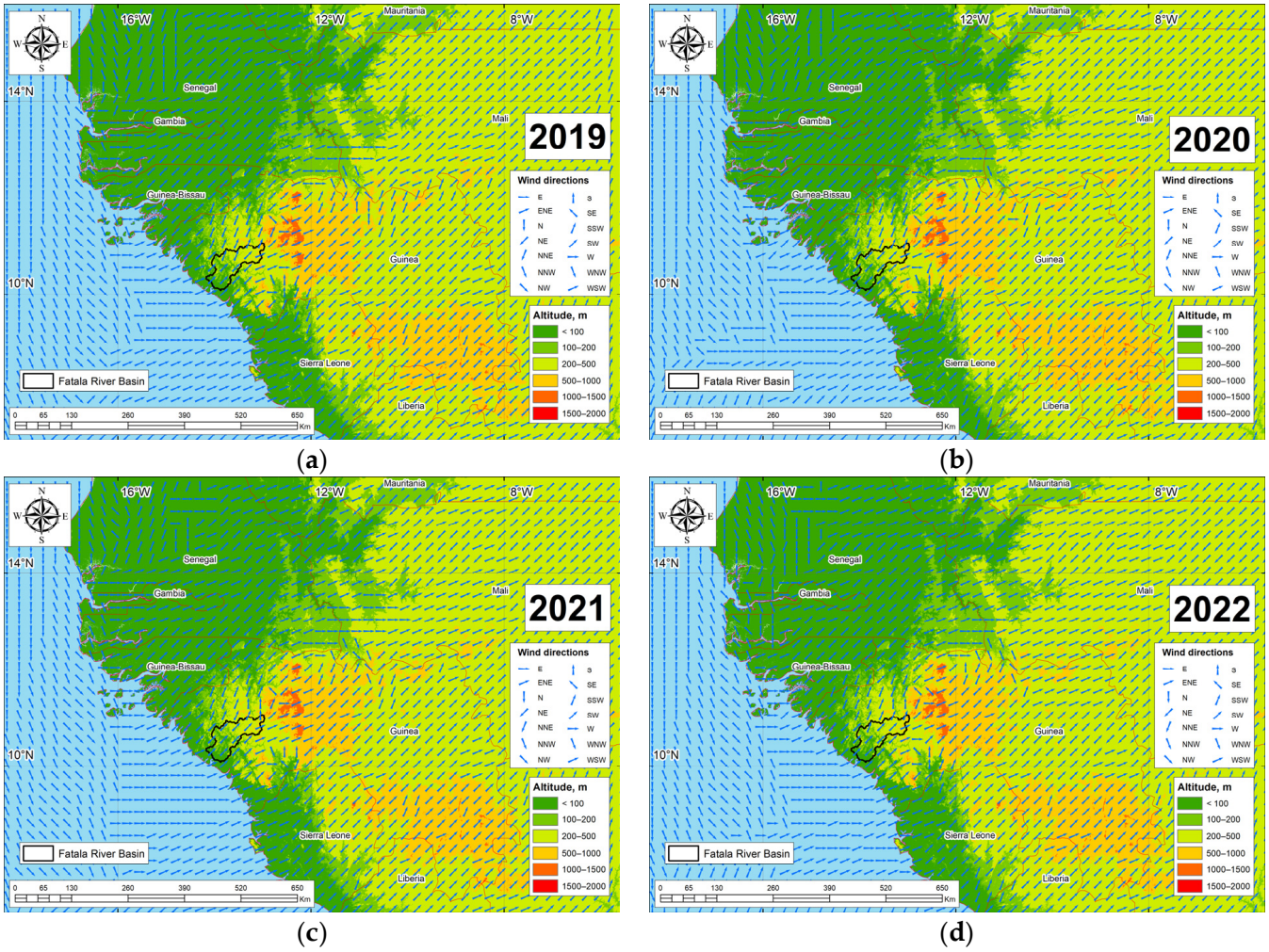

Figure 6. Prevailing wind directions in the Republic of Guinea and neighboring countries in 2019–2022: (**a**) 2019; (**b**) 2020; (**c**) 2021; (**d**) 2022.

However, when comparing the concentrations of chemical substances obtained through Sentinel-5P satellite data within the Fatala River Basin to other global regions, it becomes evident that the quantified pollution levels are relatively low. For instance, Gharibvand et al. [66] reported that in Tehran, Iran, the average concentration of nitrogen dioxide in 2019 was 523 μmol/m^2, and in 2020, it was 505 μmol/m^2. In Arak, Iran, the concentration was 710 μmol/m^2 in 2019 and 56 μmol/m^2 in 2020. In comparison to the Fatala River Basin, these concentrations were approximately 25 times higher in Tehran in 2019 and 40 times higher in Arak in 2019. Comparing the data reported by Gharibvand et al. [66] for Iranian cities in 2019 and 2020, it can be observed that ozone concentrations are 1.1 times higher than those in the Fatala River Basin.

Kaplan et al. [67] indicated that in the Istanbul region of Turkey, nitrogen dioxide levels reached 127 μmol/m^2, which is six times higher than the levels observed in the Fatala

River Basin. Cakmak et al. [68] studied nitrogen dioxide concentrations in the Marmara Region of Turkey. They showed that from June 2019 to February 2020, nitrogen dioxide levels measured 83.9 μmol/m^2. During the COVID-19 related lockdown from March 2020 to June 2020, these levels decreased to 78.4 μmol/m^2. However, after the lockdown was lifted and restrictions were eased, nitrogen dioxide concentrations quickly rebounded to an average of 85.9 μmol/m^2. These values significantly exceed the nitrogen dioxide levels calculated for the Fatala River Basin.

Nugroho R.T. [69] presents data on the levels of nitrogen dioxide and carbon monoxide on the island of Java, Indonesia, utilizing Sentinel-5P satellite data. When contrasting these datasets with the findings from the Fatala River Basin, several noteworthy observations emerge. On Java Island, the concentrations of carbon monoxide in 2020 ranged from 0.021 to 0.035 mol/m^2, which are lower in comparison to the concentrations recorded within the Fatala River Basin (as delineated in Table 3). Notably, major industrial centers on Java Island exhibited diminished carbon monoxide levels (e.g., Tangerang City at 0.0346 mol/m^2, Tangerang Regency at 0.0342 mol/m^2, and West Jakarta at 0.0340 mol/m^2) in contrast to the minimum (0.038 mol/m^2) and average (0.042 mol/m^2) values witnessed within the Fatala River Basin. As for carbon dioxide, its levels on Java Island fluctuated between 1.7 and 89.7 μmol/m^2, whereas within the Fatala River Basin, they ranged from 15 to 23 μmol/m^2. Additionally, the highest concentrations of nitrogen dioxide on Java Island were observed proximate to major industrial centers or urban areas, such as South Jakarta (85.9 μmol/m^2), Central Jakarta (85.2 μmol/m^2), and West Jakarta (81 μmol/m^2), while nitrogen dioxide concentrations in other regions of Java Island remained considerably lower.

Rehmat et al. [70] conducted an assessment of nitrogen dioxide concentrations over cities in Pakistan. Their findings reveal that from May 2018 to May 2022, average nitrogen dioxide concentrations in the ambient air in Karachi ranged from 3.0 μmol/m^2 to 0.4 mol/m^2, while in Lahore, they varied from 40.0 μmol/m^2 to 0.55 mol/m^2. These levels notably exceed the calculated values for nitrogen dioxide concentrations in the Fatala River Basin.

Comparing the nitrogen dioxide values with those in the watersheds of the northwestern slope of the Crimean Mountains [63], it becomes evident that in 2019 and 2022, the Fatala River Basin exhibited lower average nitrogen dioxide concentrations compared to the Zapadnyy Bulganak, Alma, Kacha, Belbek, and Chernaya river basins, while being equivalent to the Belbek River Basin. In 2020 and 2021, the Fatala River Basin had lower nitrogen dioxide concentrations than all the river basins on the northwestern slope of the Crimean Mountains. Remarkably, within the Fatala River Basin, a more pronounced decrease in nitrogen dioxide levels was evident in 2020. In contrast to the river basins on the northwestern slope of the Crimean Mountains, the Fatala River Basin exhibited significantly lower sulfur dioxide concentrations, which were 2 to 10 times lower, for example, compared to the Zapadnyy Bulganak River Basin. Nevertheless, within the Fatala River Basin, formaldehyde concentrations were 2.0 to 2.5 times higher, and carbon monoxide concentrations were 1.2 to 1.3 times higher compared to the river basins on the northwestern slope of the Crimean Mountains (as depicted in Figure 7).

Simultaneously, the average value of the comprehensive atmospheric pollution index for the Fatala River Basin is, on average, 1.5 times higher than that of the West Bulganak, Alma, Kacha, Belbek, and Black Sea river basins.

Overall, the variations in air pollution levels from 2019 to 2022, much like global trends, were influenced by the COVID-19 pandemic [68,71–74]. The lower levels of air pollution in the Fatala River Basin can primarily be attributed to the underdeveloped industrial activities in the settlements located within the basin, along with the prevalence of mining activities within the basin itself. The pollution levels within the river basin can serve as an indicator of the level of industrial development within the studied region.

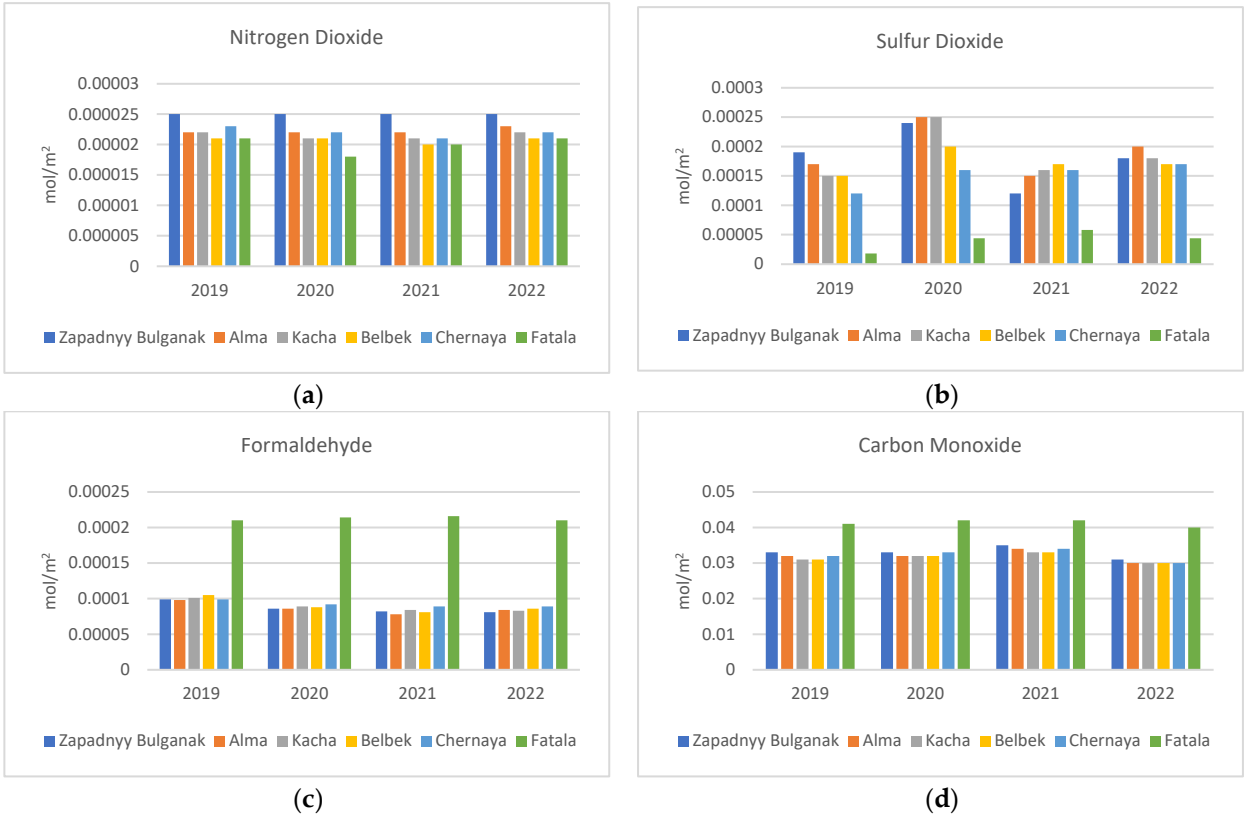

Figure 7. Comparison of average concentrations of chemical substances between the Fatala River Basin and the West Bulganak, Alma, Kacha, Belbek, and Black Sea river basins for the years 2019–2022: (**a**) Nitrogen Dioxide; (**b**) Sulfur Dioxide; (**c**) Formaldehyde; (**d**) Carbon Monoxide.

It is important to note that the analysis of pollutants and their concentrations is primarily conducted within major urban centers [69,75–77]. Studies regarding air content of various chemical elements are typically conducted at the national level, such as in Iran [75], Peru [72], Indonesia [78], India [79], Bulgaria [80], Russia [74,81], and China [82]. Specific studies on carbon monoxide concentration in the air are often associated with forest fire monitoring [83–85]. There is a significant challenge in the choice of study periods and the number of pollutants examined using Sentinel-5P satellite data in different regions of the world, making the comparison of results very complex. Additionally, the air content of various chemical elements within river basins using Sentinel-5P data has been scarcely explored [63]. Hence, there is a pressing need for intensified scientific research on air pollution within river basins in the current scenario.

This study is subject to several limitations that warrant consideration. Firstly, the analysis was confined to pollutants detected by the Sentinel-5P satellite, encompassing six key pollutants: carbon dioxide, sulfur dioxide, nitrogen dioxide, formaldehyde, methane, and ozone, all of which were considered in this study. Secondly, the temporal scope of this research was restricted to data spanning from 2019 to 2022, as provided by the Sentinel-5P satellite. Consequently, the findings are contingent on this time frame. Thirdly, it is essential to recognize that the data extracted from the Sentinel-5P satellite are measured in mol/m^2 units. There are also limitations to this study associated with the calculation of anthropogenic transformation due to the use of Landsat and Sentinel-2 satellite imagery and their spatial and temporal coverage constraints. Additionally, the methodology employed by the authors represents another limitation since it is evident that different results can be obtained with varying input datasets. The utilization of different methods for spatial data interpolation also influences the ultimate findings of the study.

Clearly, it is imperative to expand the scope of research on air pollutant analysis utilizing satellite data over time. As potential avenues for future research, the utilization

of satellite data from instruments such as GOSAT, IASI, AIRS, Tansat, and others holds promise. Another future research direction involves the use of unmanned aerial vehicle (UAV) data, which can provide a more detailed characterization of land use and more precise calculations of various anthropogenic transformation indicators.

Studying the anthropogenic transformation and air pollution within the Fatala River Basin is of great importance for achieving sustainable development for several reasons. Firstly, emissions of pollutants into the atmosphere within the river basin and the transboundary transport of air masses and pollutants from other basins can have direct and indirect impacts on human health, the state of the flora and fauna, and contribute to climate change. Therefore, the study of air pollution within river basins using remote sensing data is crucial for identifying pollution sources in near real-time and implementing measures to reduce emissions, improve air quality, and achieve sustainable development goals. Secondly, the state of the air and the development of anthropogenic activities within the Fatala River Basin directly affect the economic well-being of people living within the basin's territory. Environmental pollution can lead to economic losses, which will negatively impact the achievement of sustainable development goals in the region under study. Thirdly, studying anthropogenic transformations and air pollution allows for real-time monitoring and long-term planning that takes into account ecological and social consequences. This ensures that development projects are sustainable and do not jeopardize the well-being of future generations. Fourthly, sustainable development of the Fatala River Basin is closely linked to the United Nations Sustainable Development Goals (SDGs). Data collected from the study of anthropogenic transformations and air pollution in river basins can provide valuable information for tracking progress in achieving these global goals. Understanding anthropogenic transformations and air pollution within the river basin is fundamental to achieving sustainable development. It enables informed decision-making, protects valuable ecosystems and landscapes, promotes economic well-being, addresses climate change, and supports legal and policy measures to protect the environment and society. This has far-reaching implications for the preservation of the natural environment, society, and the economy, while providing the knowledge and data necessary for making informed decisions and taking actions to protect and enhance the well-being of current and future generations.

5. Conclusions

In this study, an assessment of anthropogenic transformation within the Fatala River Basin was conducted. Values for the coefficient of anthropogenic transformation, land degradation index, urbanity index, degree of anthropogenic transformation, and coefficient of natural protection were calculated. Based on the analysis of comprehensive data derived from processing satellite imagery from Sentinel-5P and Sentinel-2 satellites, a quantitative assessment of air concentration over the Fatala River Basin of substances such as nitrogen dioxide, sulfur dioxide, formaldehyde, methane, carbon monoxide, and ozone was presented. A series of maps depicting the degree of pollution with these chemical substances within the study area was created. Furthermore, the main centers of anthropogenic transformation located within the Fatala River Basin were examined. The central part of the Fatala River Basin was found to be subject to the highest degree of anthropogenic transformation. The main factor behind these significant anthropogenic changes is bauxite mining, along with industrial concentration near populous areas. Open-pit mining is prevalent, leading to deforestation, landscape alteration, and dust emissions. Bauxite mining itself does not heavily contribute to air pollution. Air pollution in the Fatala River Basin is not significantly correlated with anthropogenic changes. Instead, it is mainly influenced by polluted air from other regions through transboundary transport.

Author Contributions: Conceptualization, V.T., R.G. and T.G.; methodology, V.T. and R.G.; software, V.T.; validation, V.T., V.V. and T.G.; formal analysis, V.T.; investigation, V.T., R.G., N.B., N.M., V.V. and T.G.; resources, V.T.; data curation, V.T.; writing—original draft preparation, V.T.; writing—review and editing, V.T., R.G. and T.G.; visualization, V.T.; supervision, R.G.; project administration, V.V. All authors have read and agreed to the published version of the manuscript.

Funding: The work was carried out with the financial support of the Project of the Russian Federation represented by the Ministry of Science and Higher Education of the Russian Federation: a grant in the form of subsidies in accordance with paragraph 4 of Article 78.1 of the Budget Code of the Russian Federation (Agreement № 075-15-2023-592 on the topic № 13.2251.21.0216).

Institutional Review Board Statement: Not applicable.

Informed Consent Statement: Not applicable.

Data Availability Statement: The data presented in this study are available on request from the corresponding author.

Conflicts of Interest: The authors declare no conflict of interest.

Appendix A

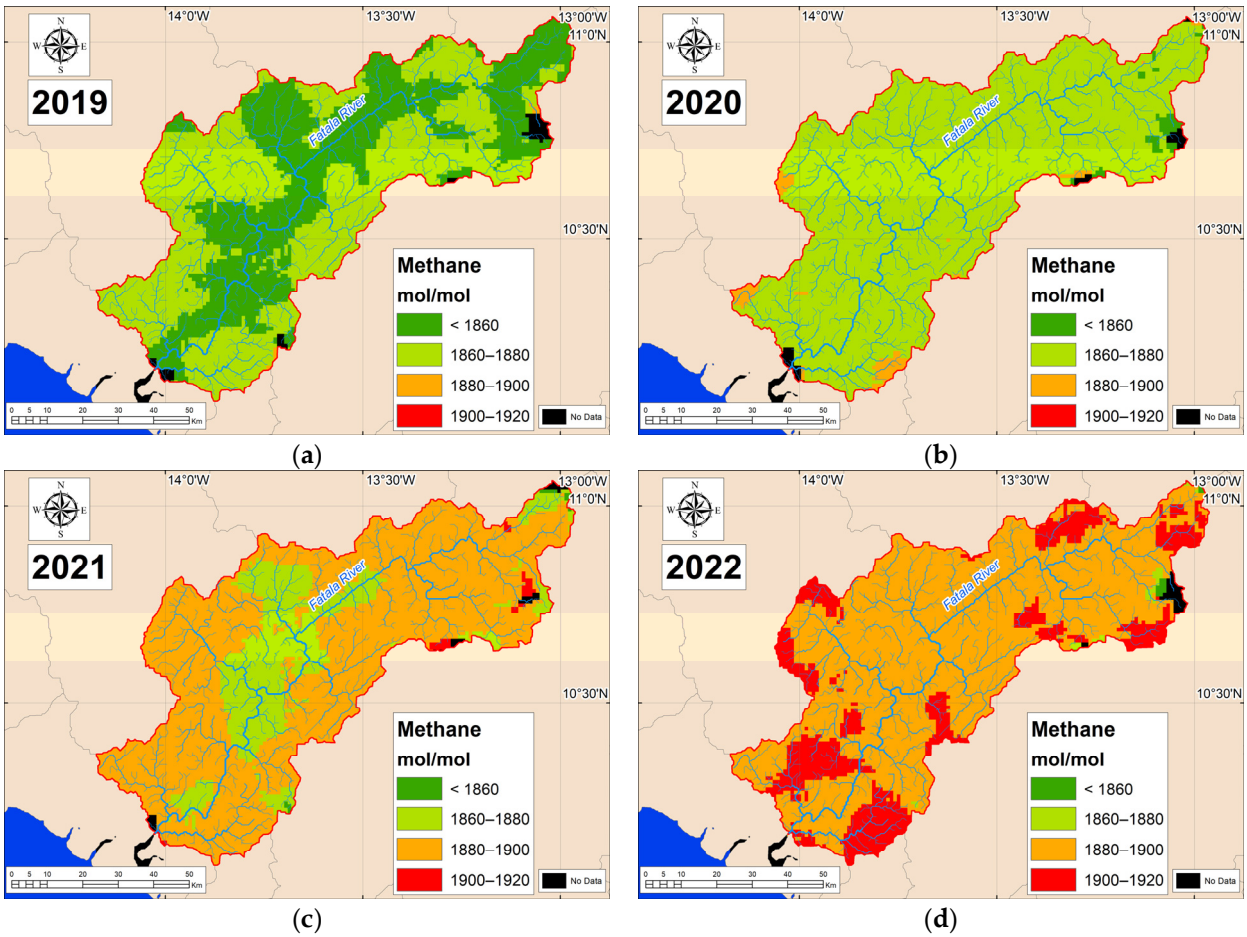

Figure A1. Distribution of methane (CH_4) content in the atmosphere in the Fatala River Basin: (**a**) 2019; (**b**) 2020; (**c**) 2021; (**d**) 2022.

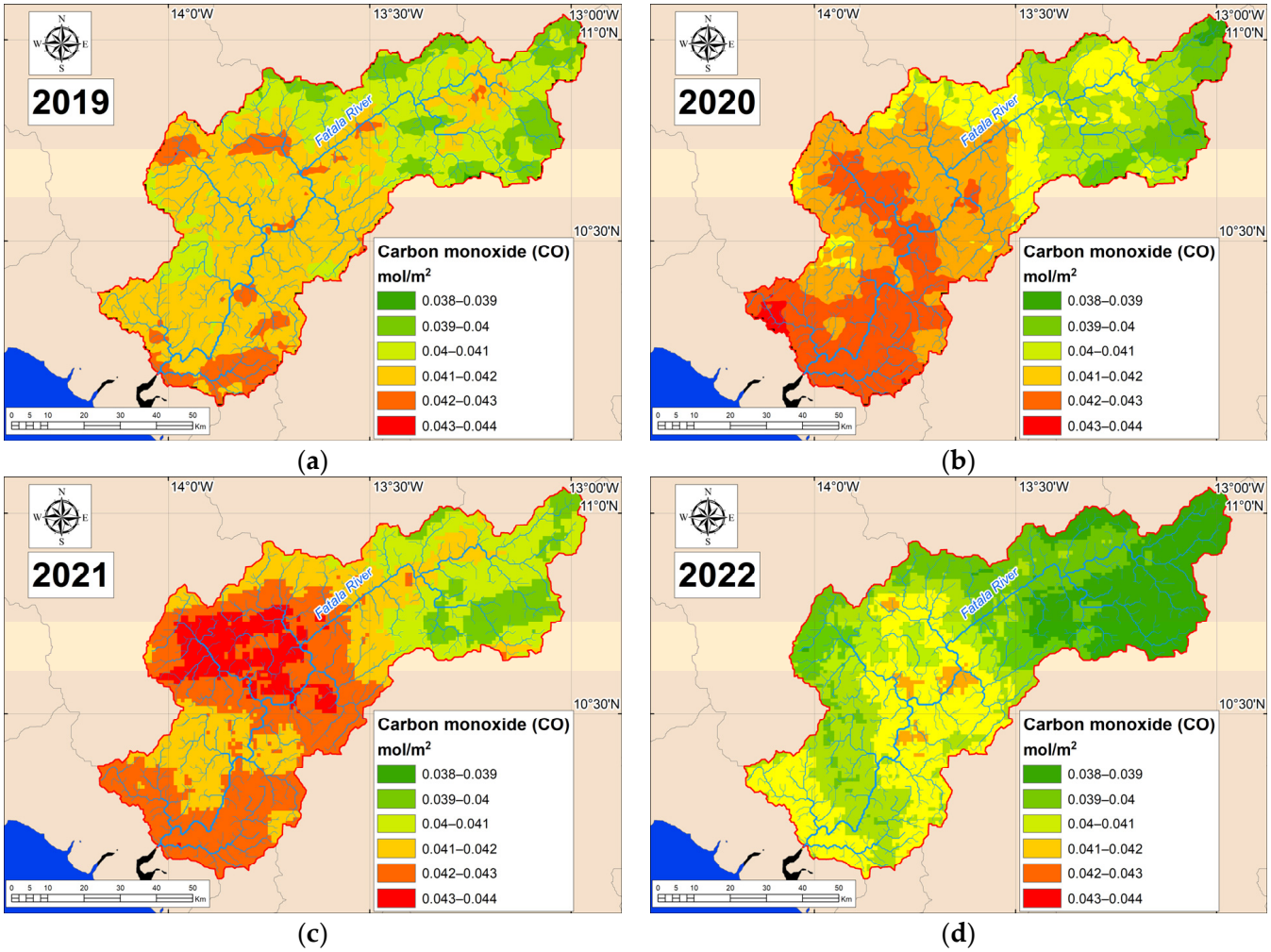

Figure A2. Distribution of carbon monoxide (CO) content in the atmosphere in the Fatala River Basin: (**a**) 2019; (**b**) 2020; (**c**) 2021; (**d**) 2022.

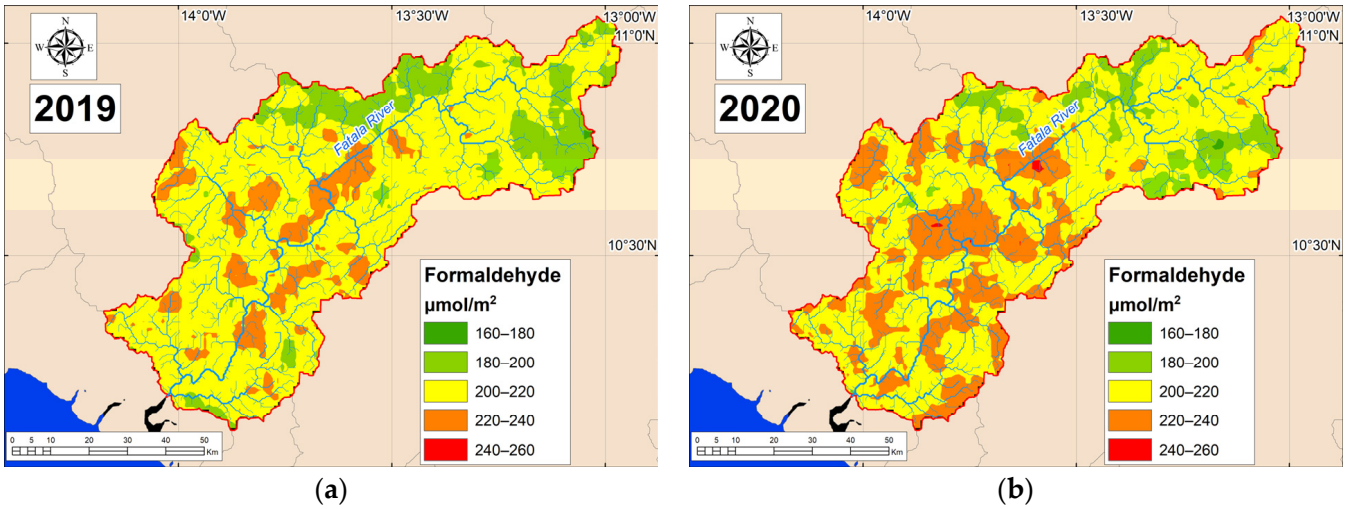

Figure A3. *Cont.*

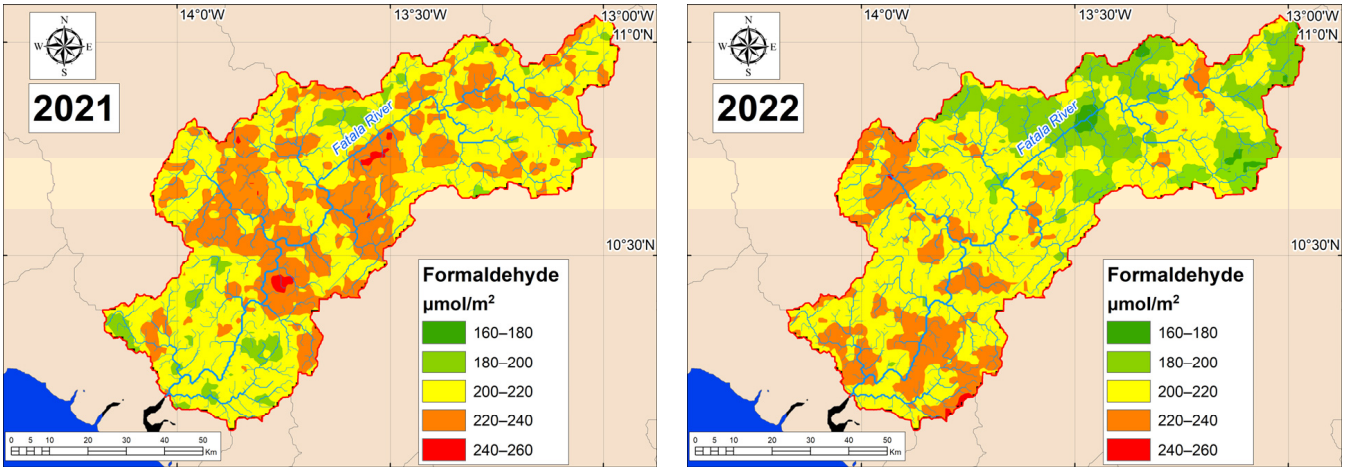

(**c**) (**d**)

Figure A3. Distribution of formaldehyde (HCHO) content in the atmosphere in the Fatala River Basin: (**a**) 2019; (**b**) 2020; (**c**) 2021; (**d**) 2022.

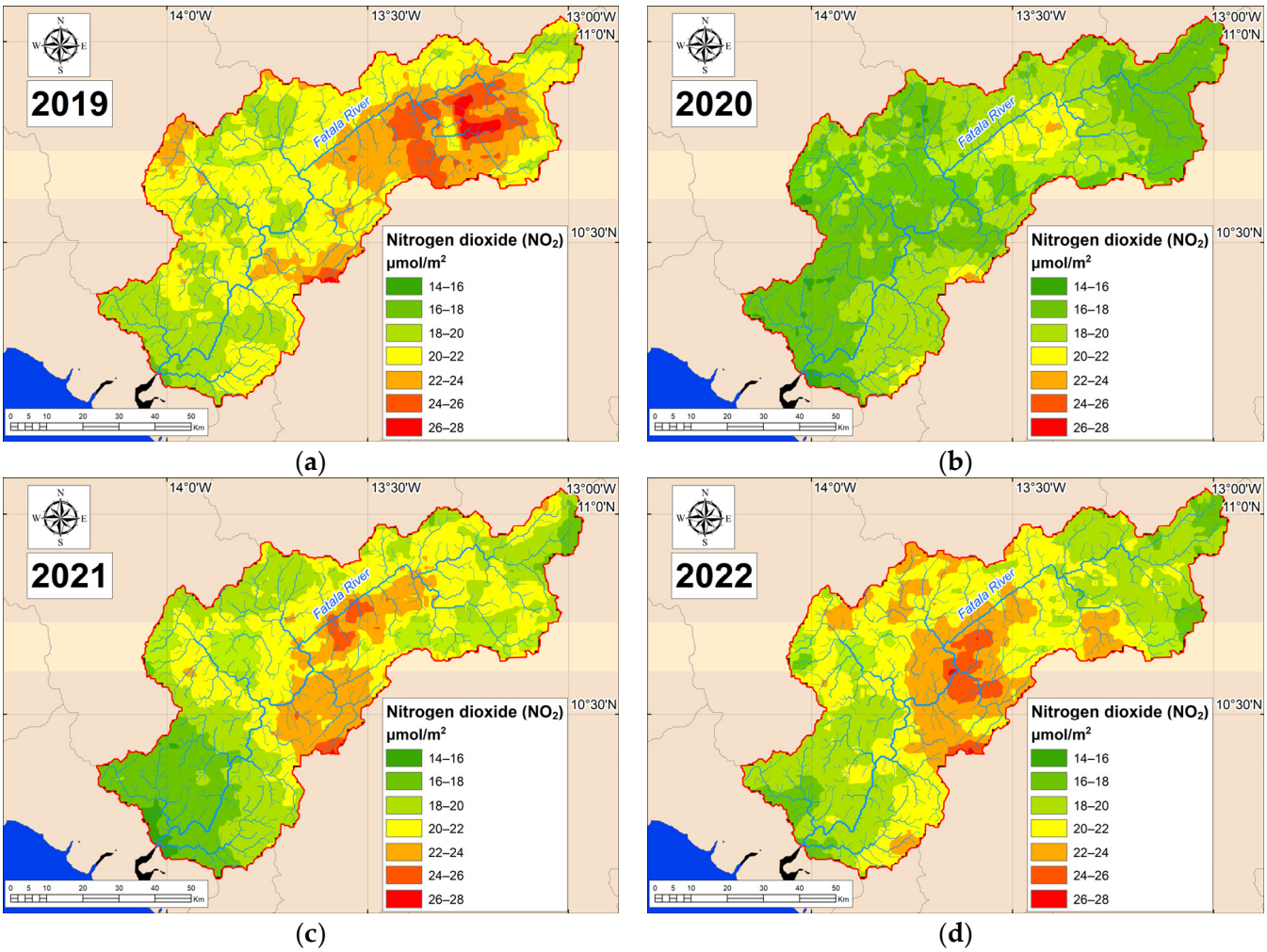

(**a**) (**b**)

(**c**) (**d**)

Figure A4. Distribution of nitrogen dioxide (NO_2) content in the atmosphere in the Fatala River Basin: (**a**) 2019; (**b**) 2020; (**c**) 2021; (**d**) 2022.

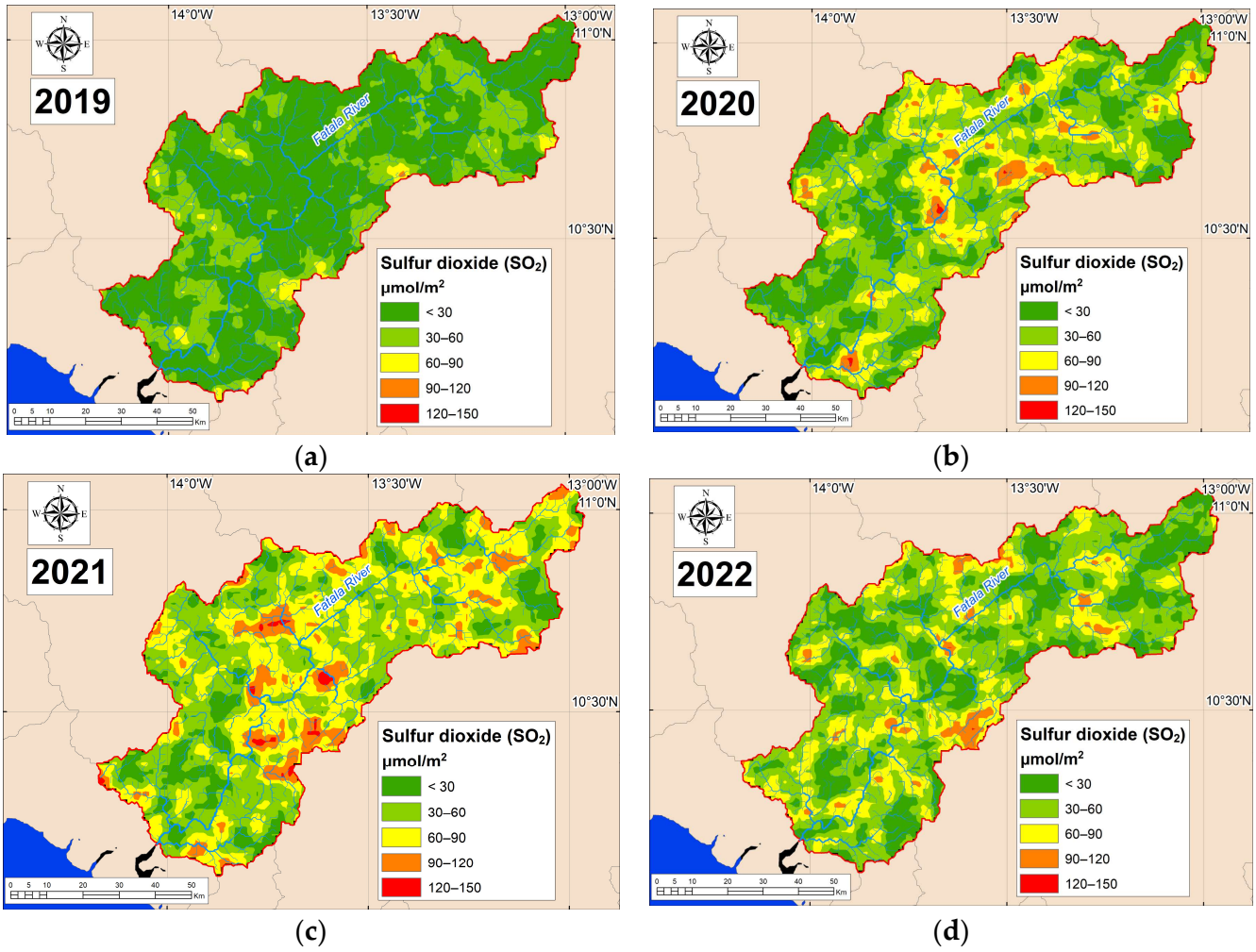

Figure A5. Distribution of sulfur dioxide (SO_2) content in the atmosphere in the Fatala River Basin: (**a**) 2019; (**b**) 2020; (**c**) 2021; (**d**) 2022.

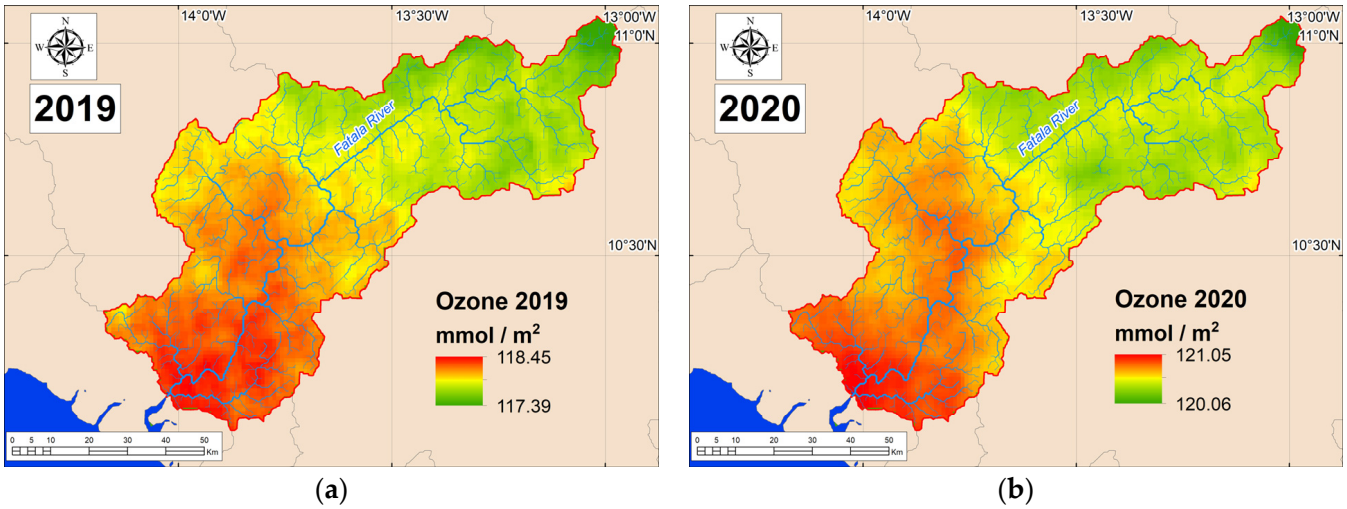

Figure A6. *Cont.*

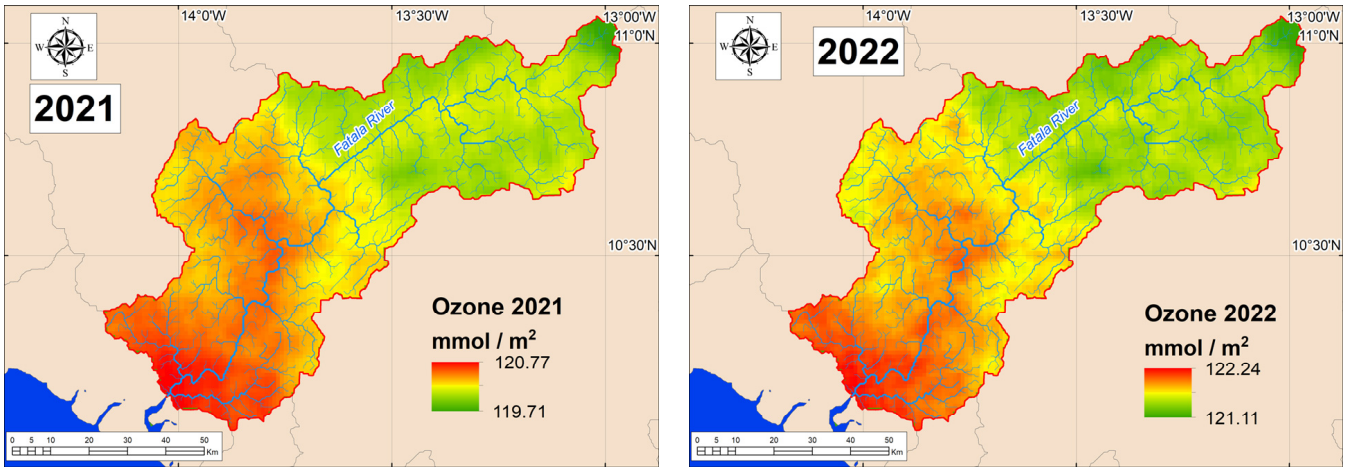

(**c**) (**d**)

Figure A6. Distribution of ozone (O_3) content in the atmosphere in the Fatala River Basin: (**a**) 2019; (**b**) 2020; (**c**) 2021; (**d**) 2022.

Appendix B

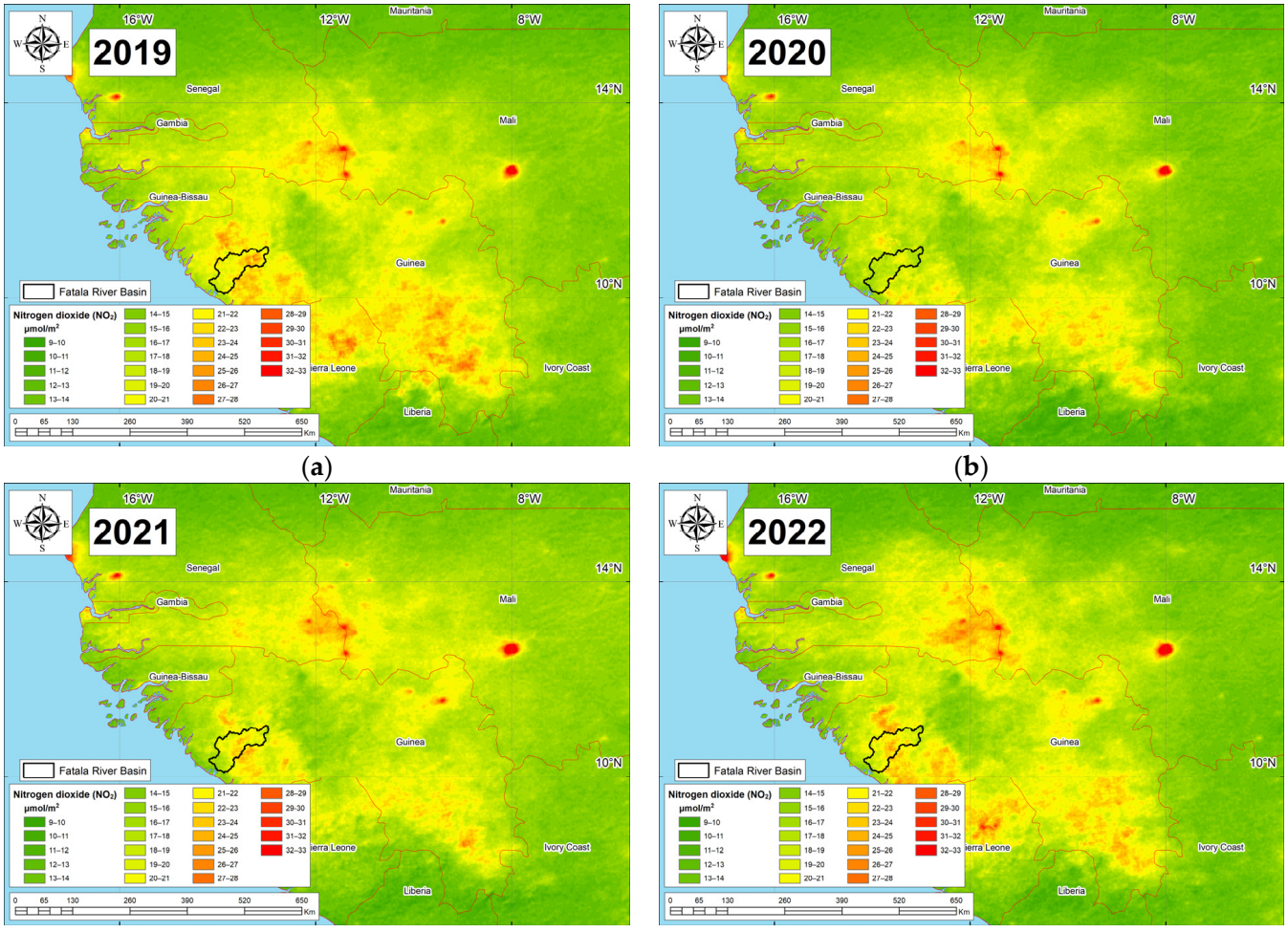

(**a**) (**b**)

(**c**) (**d**)

Figure A7. Distribution of nitrogen dioxide (NO_2) content in the atmosphere in the Republic of Guinea and neighboring countries: (**a**) 2019; (**b**) 2020; (**c**) 2021; (**d**) 2022.

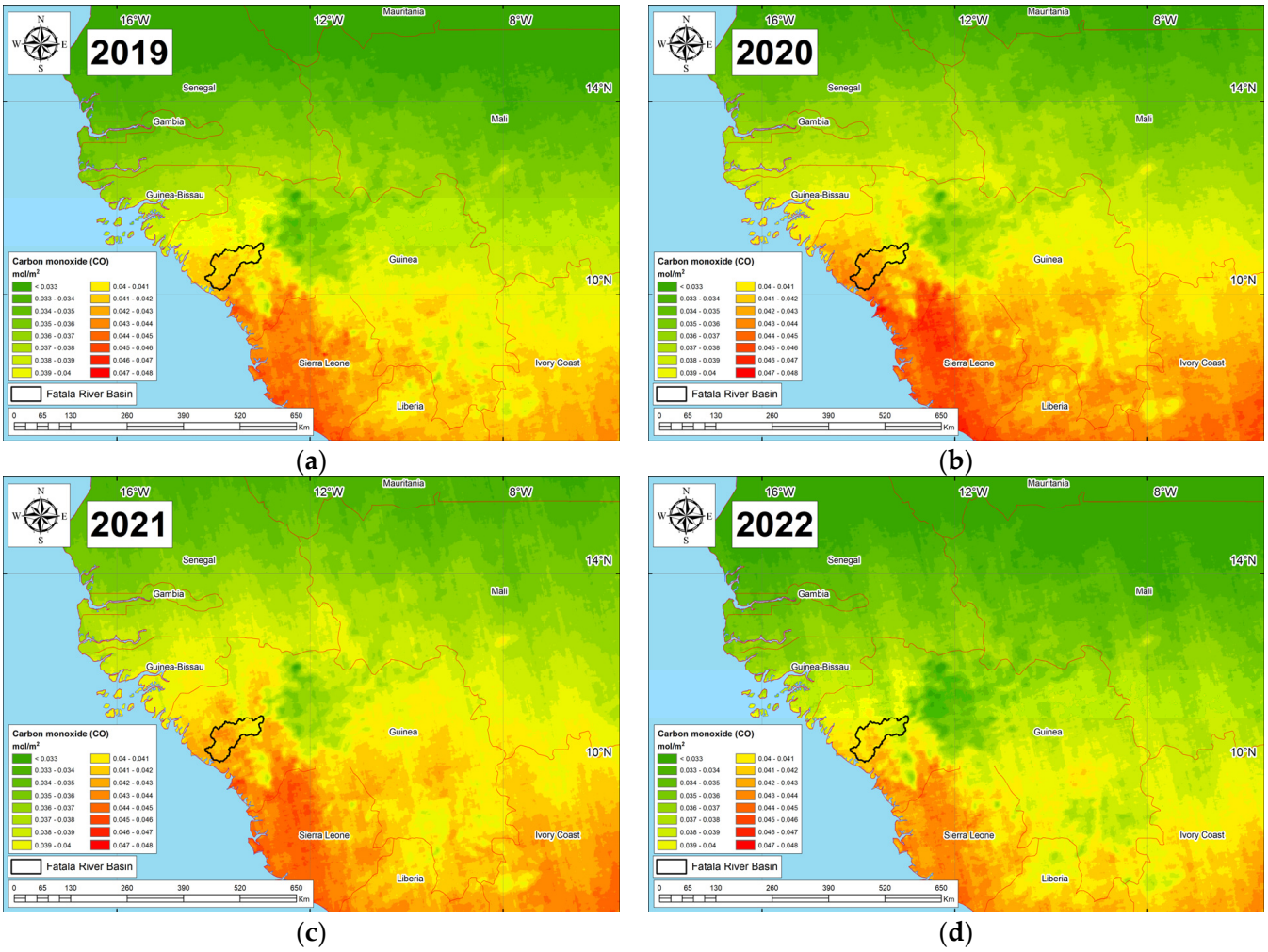

Figure A8. Distribution of carbon monoxide (CO) content in the atmosphere in the Republic of Guinea and neighboring countries: (**a**) 2019; (**b**) 2020; (**c**) 2021; (**d**) 2022.

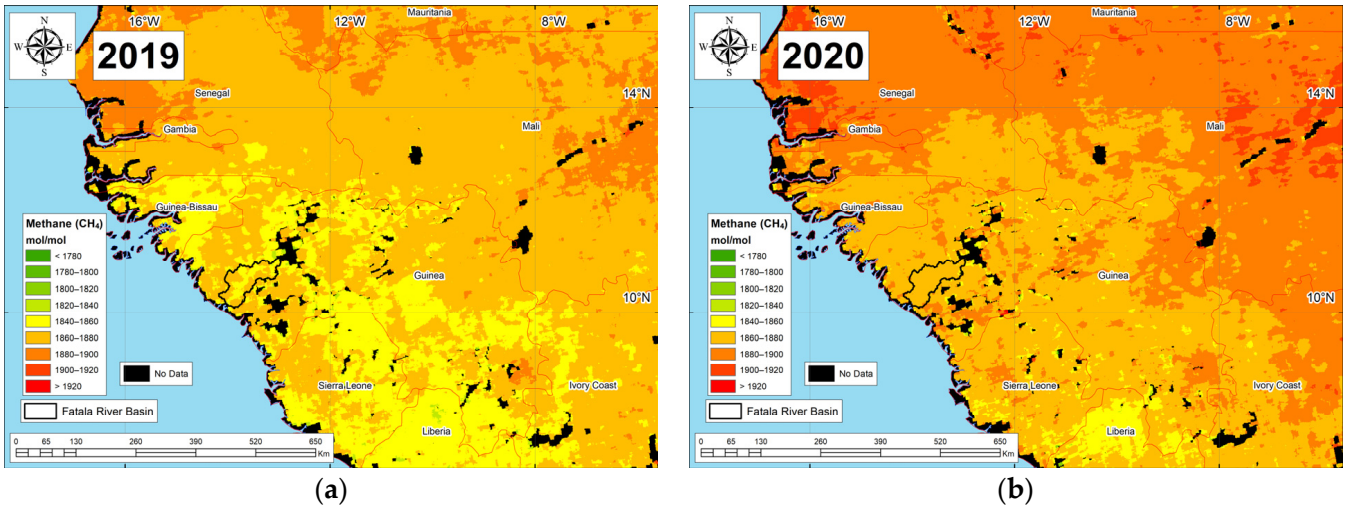

Figure A9. *Cont.*

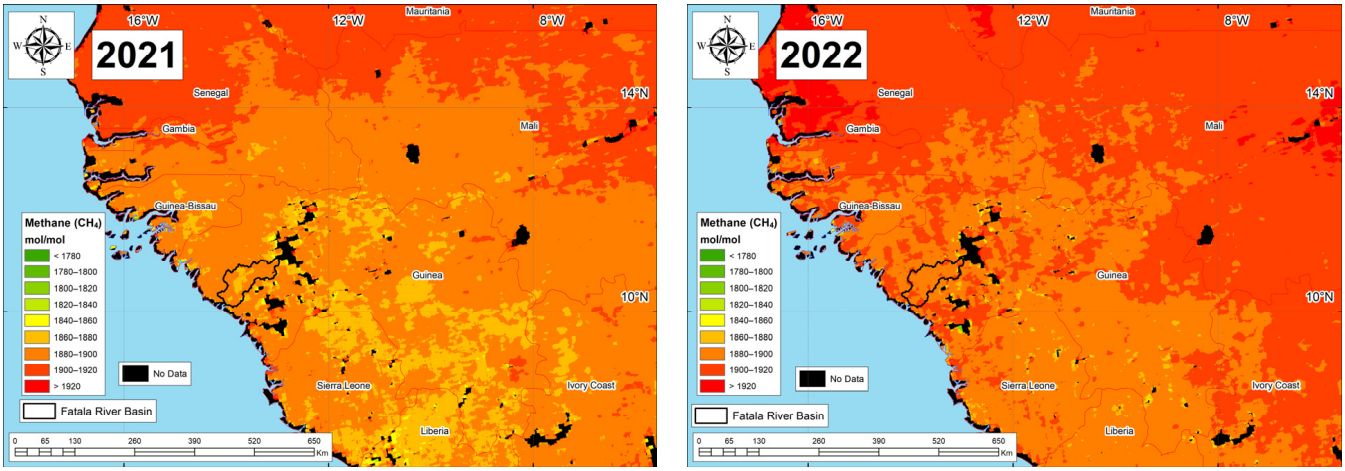

(**c**) (**d**)

Figure A9. Distribution of methane (CH_4) content in the atmosphere in the Republic of Guinea and neighboring countries: (**a**) 2019; (**b**) 2020; (**c**) 2021; (**d**) 2022.

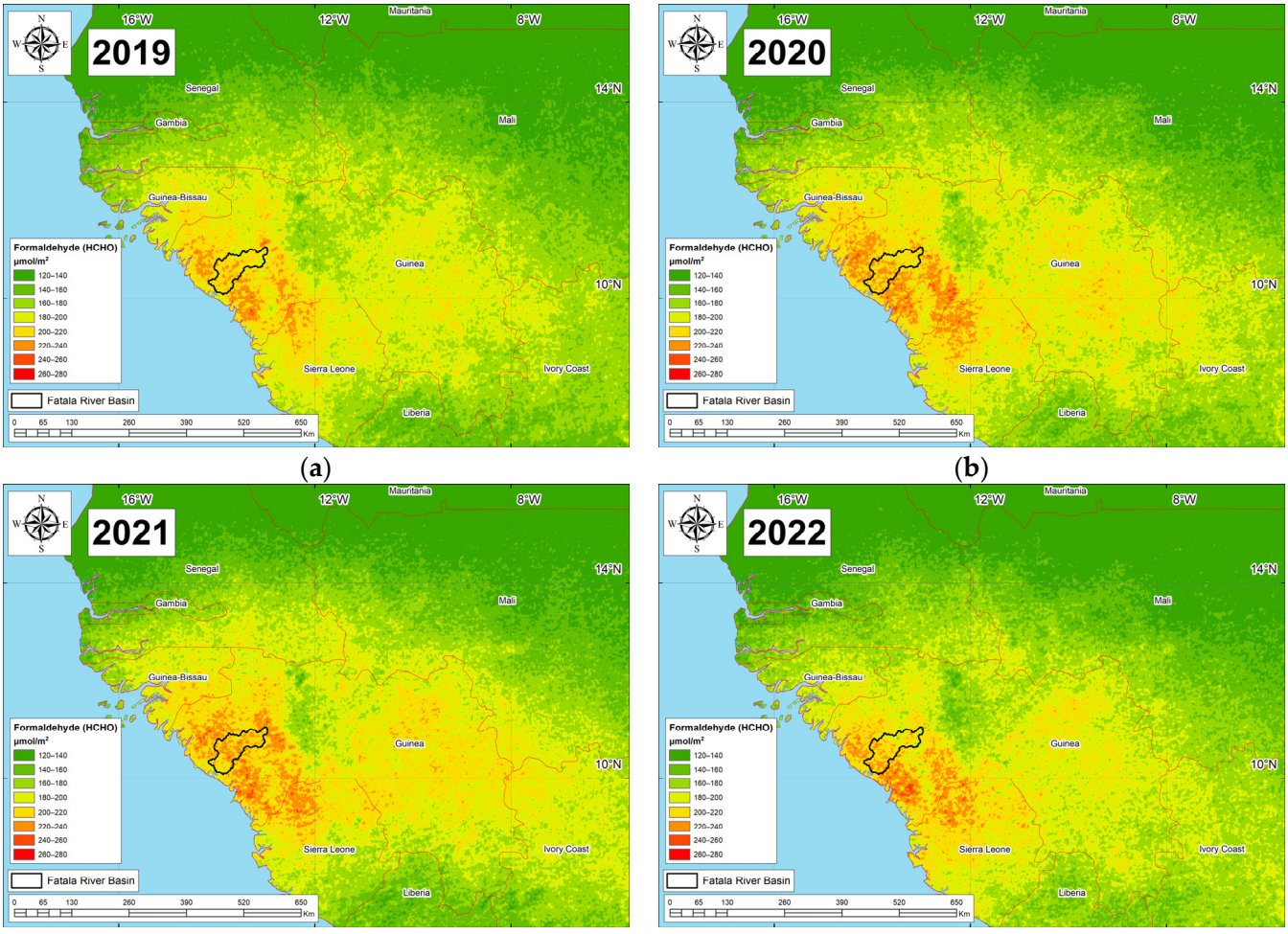

(**a**) (**b**)

(**c**) (**d**)

Figure A10. Distribution of formaldehyde (HCHO) content in the atmosphere in the Republic of Guinea and neighboring countries: (**a**) 2019; (**b**) 2020; (**c**) 2021; (**d**) 2022.

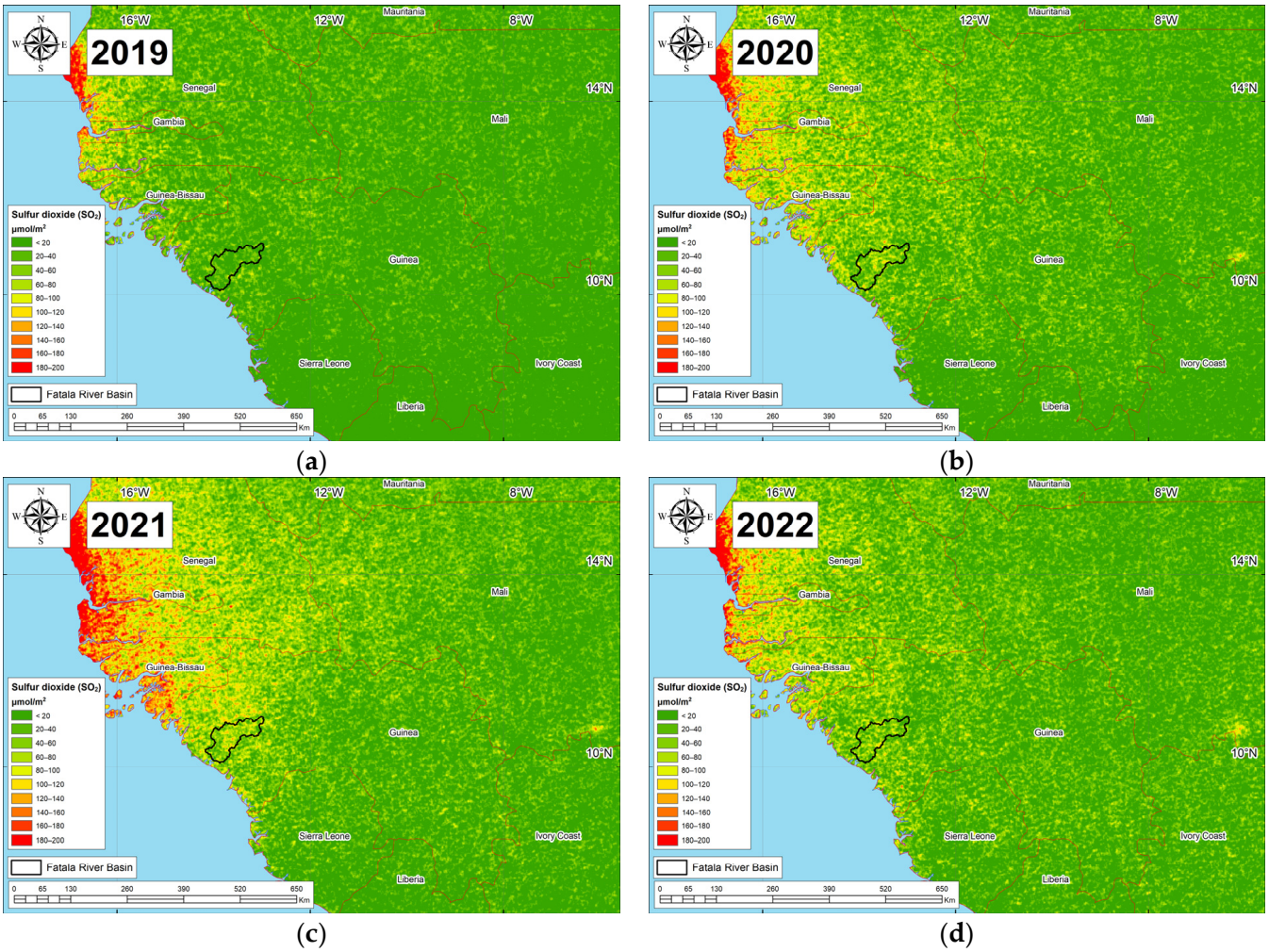

Figure A11. Distribution of sulfur dioxide (SO_2) content in the atmosphere in the Republic of Guinea and neighboring countries: (**a**) 2019; (**b**) 2020; (**c**) 2021; (**d**) 2022.

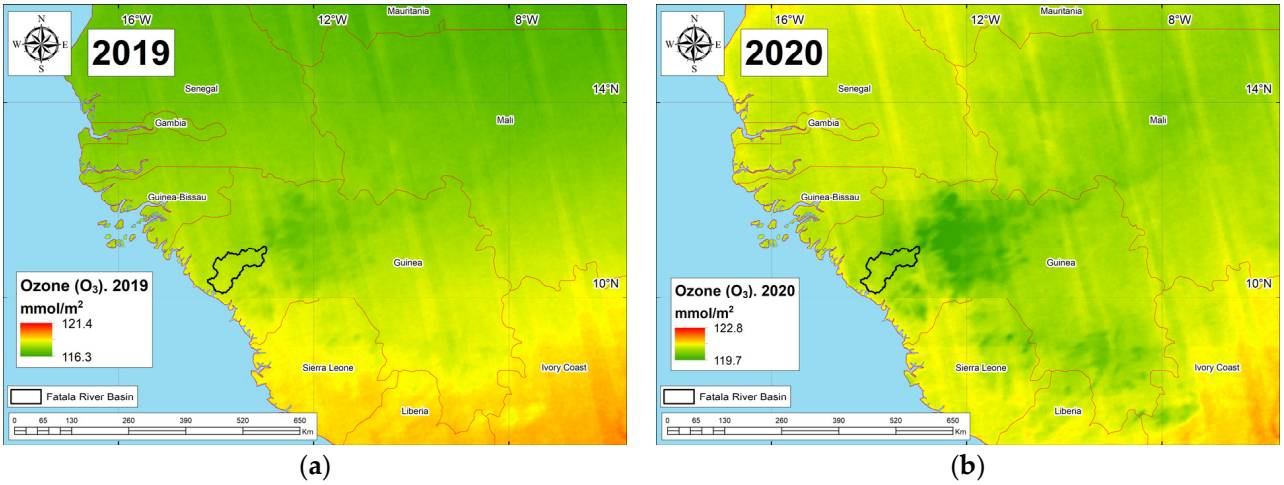

Figure A12. *Cont*.

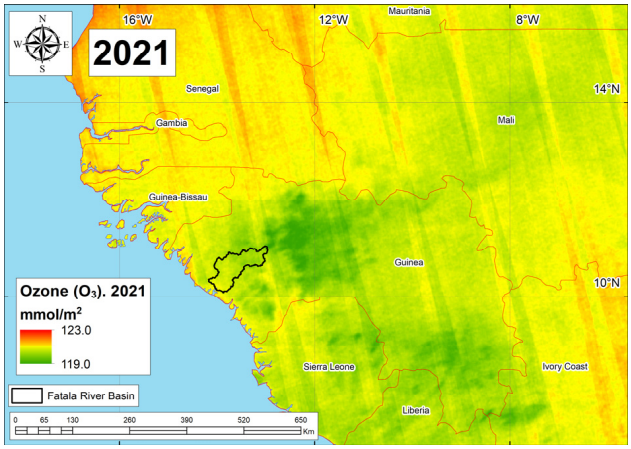

(**c**)

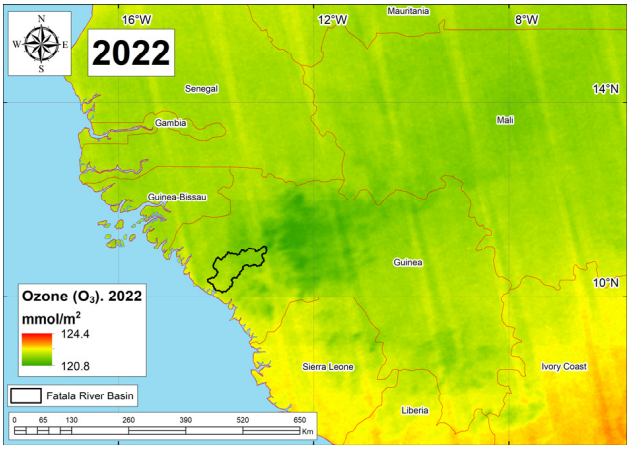

(**d**)

Figure A12. Distribution of ozone (O_3) content in the atmosphere in the Republic of Guinea and neighboring countries: (**a**) 2019; (**b**) 2020; (**c**) 2021; (**d**) 2022.

Appendix C

Table A1. Distribution of mean pollutant concentrations across altitudinal ranges in the Fatala River Basin in 2019.

Altitude, m	Pollutant					
	Methane, mol/mol	Carbon Monoxide, mol/m^2	Ozone, mol/m^2	Formaldehyde, mol/m^2	Nitrogen Dioxide, mol/m^2	Sulfur Dioxide, mol/m^2
0–100	1862.2	0.0418	0.1183	0.000214	0.0000199	0.0000146
100–200	1860.6	0.0415	0.1182	0.000214	0.0000208	0.0000190
200–300	1860.5	0.0412	0.1180	0.000211	0.0000216	0.0000201
300–400	1860.2	0.0406	0.1179	0.000205	0.0000221	0.0000200
400–500	1860.4	0.0403	0.1179	0.000203	0.0000226	0.0000189
500–600	1856.1	0.0401	0.1178	0.000202	0.0000216	0.0000134
600–700	1854.5	0.0397	0.1178	0.000196	0.0000214	0.0000217
700–800	1847.6	0.0396	0.1176	0.000200	0.0000205	0.0000180
800–900	1845.5	0.0393	0.1175	0.000200	0.0000203	0.0000155
900–1000	1845.4	0.0394	0.1175	0.000196	0.0000212	0.0000000
1000–1025	1823.4	0.0389	0.1174	0.000204	0.0000206	0.0000000

Table A2. Distribution of mean pollutant concentrations across altitudinal ranges in the Fatala River Basin in 2020.

Altitude, m	Pollutant					
	Methane, mol/mol	Carbon Monoxide, mol/m^2	Ozone, mol/m^2	Formaldehyde, mol/m^2	Nitrogen Dioxide, mol/m^2	Sulfur Dioxide, mol/m^2
0–100	1873.5	0.0433	0.1208	0.000218	0.0000178	0.0000410
100–200	1873.5	0.0428	0.1207	0.000218	0.0000179	0.0000424
200–300	1873.0	0.0421	0.1206	0.000215	0.0000183	0.0000483
300–400	1872.7	0.0411	0.1205	0.000207	0.0000186	0.0000483
400–500	1872.5	0.0405	0.1205	0.000206	0.0000184	0.0000444
500–600	1869.2	0.0398	0.1205	0.000206	0.0000176	0.0000390
600–700	1864.1	0.0396	0.1205	0.000202	0.0000174	0.0000274
700–800	1864.9	0.0392	0.1203	0.000207	0.0000173	0.0000190
800–900	1871.1	0.0389	0.1202	0.000207	0.0000169	0.0000018
900–1000	1882.5	0.0387	0.1201	0.000208	0.0000163	0.0000128
1000–1025	No Data	0.0383	0.1201	0.000206	0.0000160	0.0000144

Table A3. Distribution of mean pollutant concentrations across altitudinal ranges in the Fatala River Basin in 2021.

Altitude, m	Pollutant					
	Methane, mol/mol	Carbon Monoxide, mol/m^2	Ozone, mol/m^2	Formaldehyde, mol/m^2	Nitrogen Dioxide, mol/m^2	Sulfur Dioxide, mol/m^2
0–100	1883.3	0.0425	0.1205	0.000214	0.0000186	0.0000559
100–200	1881.9	0.0425	0.1204	0.000219	0.0000202	0.0000602
200–300	1882.4	0.0420	0.1204	0.000218	0.0000209	0.0000609
300–400	1883.8	0.0410	0.1203	0.000215	0.0000206	0.0000580
400–500	1886.2	0.0405	0.1202	0.000215	0.0000202	0.0000595
500–600	1885.4	0.0401	0.1202	0.000212	0.0000194	0.0000583
600–700	1884.0	0.0401	0.1202	0.000214	0.0000197	0.0000424
700–800	1869.3	0.0399	0.1200	0.000211	0.0000191	0.0000424
800–900	1860.8	0.0396	0.1198	0.000213	0.0000191	0.0000716
900–1000	No Data	0.0393	0.1198	0.000209	0.0000187	0.0000947
1000–1025	No Data	0.0391	0.1197	0.000212	0.0000190	0.0000829

Table A4. Distribution of mean pollutant concentrations across altitudinal ranges in the Fatala River Basin in 2022.

Altitude, m	Pollutant					
	Methane, mol/mol	Carbon Monoxide, mol/m^2	Ozone, mol/m^2	Formaldehyde, mol/m^2	Nitrogen Dioxide, mol/m^2	Sulfur Dioxide, mol/m^2
0–100	1898.3	0.0412	0.1220	0.000218	0.0000201	0.0000456
100–200	1896.8	0.0408	0.1219	0.000215	0.0000212	0.0000445
200–300	1896.3	0.0402	0.1218	0.000209	0.0000215	0.0000458
300–400	1896.9	0.0393	0.1216	0.000203	0.0000205	0.0000463
400–500	1897.1	0.0386	0.1216	0.000200	0.0000202	0.0000427
500–600	1895.4	0.0381	0.1216	0.000197	0.0000189	0.0000319
600–700	1886.7	0.0377	0.1216	0.000199	0.0000190	0.0000380
700–800	1887.3	0.0373	0.1214	0.000194	0.0000174	0.0000299
800–900	1871.3	0.0371	0.1213	0.000199	0.0000178	0.0000127
900–1000	1880.3	0.0371	0.1212	0.000204	0.0000177	0.0000054
1000–1025	1857.4	0.0366	0.1212	0.000189	0.0000183	0.0000026

References

1. Ji, L.; Li, Y.; Zhang, G.; Bi, Y. Anthropogenic Disturbances Have Contributed to Degradation of River Water Quality in Arid Areas. *Water* **2021**, *13*, 3305. [CrossRef]
2. Rothacker, L.; Dosseto, A.; Francke, A.; Chivas, A.R.; Vigier, N.; Kotarba-Morley, A.M.; Menozzi, D. Impact of climate change and human activity on soil landscapes over the past 12,300 years. *Sci. Rep.* **2018**, *8*, 247. [CrossRef] [PubMed]
3. Feist, B.E.; Levin, P.S. Novel Indicators of Anthropogenic Influence on Marine and Coastal Ecosystems. *Front. Mar. Sci.* **2016**, *3*, 113. [CrossRef]
4. Vodolazhskij, A.N.; Serikov, M.T. The determinations of values of reduce of forest recreation resources due to anthropogenic influence. *For. Eng. J.* **2014**, *3*, 70–76. [CrossRef]
5. Cahyaningsih, A.P.; Deanova, A.K.; Pristiawati, C.M.; Ulumuddin, Y.I.; Kusumawati, L.; Setyawan, A.D. Review: Causes and impacts of anthropogenic activities on mangrove deforestation and degradation in Indonesia. *Int. J. Bonorowo Wetl.* **2022**, *12*, 12–22. [CrossRef]
6. Rokhim, R.; Adawiyah, W.; Nasution, R.E.F. The negative impact of coal mining company on health, environment, climate change, economic sustainability and macroeconomic. *E3S Web Conf.* **2018**, *74*, 01004. [CrossRef]
7. Sudarmo, S. Towards collective action in conflict resolution on environmental impacts due to coal mining in Indonesia. *IOP Conf. Ser. Earth Environ. Sci.* **2021**, *905*, 012105. [CrossRef]
8. Ugochukwu, U.C.; Onuora, O.H.; Kurumeh, L.; Mbakwe, U.I.; Okolo, O.J.; Onuorah, A.L. Pollution of Ekulu River in Enugu: A Case of Negative Human Impact on the Environment. *IOSR J. Environ. Sci. Toxicol. Food Technol.* **2014**, *8*, 83–92. [CrossRef]
9. Bespalova, E.V.B. Inventory of the Voronezh Reservoir Anthropogenic Pollution Sources. *Water Sect. Russ. Probl. Technol. Manag.* **2019**, 78–84. [CrossRef]

10. de Sousa, C.A.F.; da Silveira, J.A.R.; Santos, C.A.G.; da Silva, R.M. A methodological proposal to analyze urban sprawl, negative environmental impacts, and land degradation in the case of João Pessoa City (Brazil) between 1991 and 2018. *Environ. Monit. Assess.* **2023**, *195*, 738. [CrossRef]
11. Ouseley-Torrezao, E. An analysis of the impact of Globalization and Economic Adjustment on Urban Governance. *J. Public Adm. Gov.* **2013**, *3*, 15. [CrossRef]
12. Archibald, A.T.; Folberth, G.; Wade, D.C.; Scott, D. A world avoided: Impacts of changes in anthropogenic emissions on the burden and effects of air pollutants in Europe and North America. *Faraday Discuss.* **2017**, *200*, 475–500. [CrossRef] [PubMed]
13. Yao, H.; Wang, L.; Liu, Y.; Zhou, J.; Lu, J. Impact of the COVID-19 lockdown on typical ambient air pollutants: Cyclical response to anthropogenic emission reduction. *Heliyon* **2023**, *9*, e15799. [CrossRef]
14. Manojlović, S.; Antić, M.; Šantić, D.; Sibinović, M.; Carević, I.; Srejić, T. Anthropogenic Impact on Erosion Intensity: Case Study of Rural Areas of Pirot and Dimitrovgrad Municipalities, Serbia. *Sustainability* **2018**, *10*, 826. [CrossRef]
15. Depountis, N.; Michalopoulou, M.; Kavoura, K.; Nikolakopoulos, K.; Sabatakakis, N. Estimating Soil Erosion Rate Changes in Areas Affected by Wildfires. *ISPRS Int. J. Geo-Inform.* **2020**, *9*, 562. [CrossRef]
16. Agbola, B.S.; Ajayi, O.; Taiwo, O.J.; Wahab, B.W. The August 2011 flood in Ibadan, Nigeria: Anthropogenic causes and consequences. *Int. J. Disaster Risk Sci.* **2012**, *3*, 207–217. [CrossRef]
17. Villarini, G.; Zhang, W.; Quintero, F.; Krajewski, W.F.; Vecchi, G.A. Attribution of the impacts of the 2008 flooding in Cedar Rapids (Iowa) to anthropogenic forcing. *Environ. Res. Lett.* **2020**, *15*, 114057. [CrossRef]
18. Zaalishvili, V.; Melkov, D.; Dobrev, N.; Kanukov, A. Integrated monitoring of slope processes in North Ossetia. *E3S Web Conf.* **2021**, *281*, 09030. [CrossRef]
19. Stepnova, Y.A.; Stepnov, A.A.; Konovalov, A.V.; Gensiorovskiy, Y.V.; Lobkina, V.A.; Muzychenko, L.E.; Muzychenko, A.A.; Orekhov, A.A. Predictive Model of Rainfall-Induced Landslides in High-Density Urban Areas of the South Primorsky Region (Russia). *Pure Appl. Geophys.* **2021**, *179*, 4013–4024. [CrossRef]
20. Sheuyange, A.; Oba, G.; Weladji, R.B. Effects of anthropogenic fire history on savanna vegetation in northeastern Namibia. *J. Environ. Manag.* **2005**, *75*, 189–198. [CrossRef]
21. Dey, D.C.; Guyette, R.P. Anthropogenic fire history and red oak forests in south-central Ontario. *For. Chron.* **2000**, *76*, 339–347. [CrossRef]
22. Kalugin, A.S.; Lupakov, S.Y. The Effect of Natural and Anthropogenic Climate Changes on River Runoff and Snow Water Equivalent in the Lena River Basin. *Water Resour.* **2023**, *50*, 557–568. [CrossRef]
23. Tishkov, A.A. Biogeographical consequences of natural and anthropogenic climate changes. *Biol. Bull. Rev.* **2012**, *2*, 132–140. [CrossRef]
24. Popović, B.; Šoja, S.J.; Paunović, T.; Maletić, R. Evaluation of Sustainable Development Management in EU Countries. *Sustainability* **2019**, *11*, 7140. [CrossRef]
25. Fortuński, B. Sustainable Development and Energy Policy: Actual CO2 Emissions in the European Union in the Years 1997–2017, Considering Trade with China and the USA. *Sustainability* **2020**, *12*, 3363. [CrossRef]
26. Alao, A. *Natural Resources and Conflict in Africa: The Tragedy of Endowment*; University Rochester Press: Rochester, NY, USA, 2007; Volume 29.
27. Li, X.; Lei, S.; Liu, Y.; Chen, H.; Zhao, Y.; Gong, C.; Bian, Z.; Lu, X. Evaluation of Ecological Stability in Semi-Arid Open-Pit Coal Mining Area Based on Structure and Function Coupling during 2002–2017. *Remote Sens.* **2021**, *13*, 5040. [CrossRef]
28. Zakonnova, L.; Babenko, A.; Nikishkin, I.; Idrisheva, Z.; Minasyan, R. Integrated approach to solving the problems of land recovery and disposal of solid waste in the coal mining region. *E3S Web Conf.* **2021**, *315*, 02009. [CrossRef]
29. Hota, P.; Behera, B. Opencast coal mining and sustainable local livelihoods in Odisha, India. *Miner. Econ.* **2016**, *29*, 1–13. [CrossRef]
30. Oshionebo, E. *Mineral Mining in Africa*; Taylor & Francis Ltd.: London, UK, 2020. [CrossRef]
31. Kolie, B.; Yao, J.; Sunahara, G.; Duonamou, L. Environmental Impact of Lefa Gold Mining on Its Local Population, Republic of Guinea. *Nat. Resour.* **2019**, *10*, 305–323. [CrossRef]
32. Sidibé, D.; Konaté, A.A.; Kaba, O.B.; Traoré, S. Bauxite Mining Industry in Guinea and the Valorization Prospects of the Resulting Residue for Engineering Purposes. *Nov. Perspect. Eng. Res.* **2021**, *4*, 94–110. [CrossRef]
33. Kolie, B.; Jun, Y.; Sunahara, G.; Camara, M. Characterization of the rock blasting process impacts in Lefa gold mine, Republic of Guinea. *Environ. Earth Sci.* **2021**, *80*, 1–17. [CrossRef]
34. Menut, L.; Flamant, C.; Turquety, S.; Deroubaix, A.; Chazette, P.; Meynadier, R. Impact of biomass burning on pollutant surface concentrations in megacities of the Gulf of Guinea. *Atmos. Meas. Tech.* **2018**, *18*, 2687–2707. [CrossRef]
35. Abdul, W.; Oguntuase, K.; Omoniyi, I.; Bada, S.; Adekoya, E.; Bashir, A.; Ibebuike, L.; Opajobi, G. Dynamics of heavy metal Pollution in Tropical lagoon of Gulf of Guinea, West Africa. *J. Appl. Sci. Environ. Manag.* **2019**, *23*, 985. [CrossRef]
36. Borowski, P.F. Environmental pollution as a threats to the ecology and development in Guinea Conakry. *Environ. Prot. Nat. Resour.* **2017**, *28*, 27–32. [CrossRef]
37. Diallo, A.M.; Konaté, A.A.; Oularé, F.; Zaheer, M. Vulnerability of groundwater to pollution at the Dabiss bauxite mining area, Boké Prefecture, Republic of Guinea. *Geol. Ecol. Landscapes* **2022**, 1–20. [CrossRef]
38. Diallo, P. *Regime Stability, Social Insecurity and Bauxite Mining in Guinea*; Taylor & Francis Ltd.: London, UK, 2019. [CrossRef]
39. Diallo, A.K.; Conte, M.S.M.; Kaba, O.B.; Soumah, A.; Camara, M. Petrological and Statistical Studies of the Limbiko Bauxite Deposit, Republic of Guinea. *Int. J. Geosci.* **2023**, *14*, 351–376. [CrossRef]

40. Wilhelm, C.; Maconachie, R. Exploring local content in Guinea's bauxite sector: Obstacles, opportunities and future trajectories. *Resour. Policy* **2020**, *71*, 101935. [CrossRef]
41. Sanoh, O.; Zhang, Q.; Wang, D.; Aurélien, N. Guinea's Bauxite Resources Evaluation and Forecasting Using Elasticity Demand Method. *Open J. Soc. Sci.* **2022**, *10*, 400–418. [CrossRef]
42. Beavogui, M.C.; Balmaev, B.G.; Kaba, O.B.; Konaté, A.A.; Loginova, I.V. Bauxite enrichment process (Bayer process): Bauxite cases from Sangaredi (Guinea) and Sierra Leone. *AIP Conf. Proc.* **2022**, *2456*, 020003. [CrossRef]
43. Balde, M.Y.; Djangang, C.N.; Diallo, R.B.; Blanchart, P.; Njopwouo, D. Physicochemical Characterisation for Potential Uses as Industrial Mineral of Bauxite from Débélé, Guinea. *J. Mater. Sci. Chem. Eng.* **2021**, *9*, 9–22. [CrossRef]
44. Komara, M.L.; Camara, C.A.T.; Bangoura, N.N.; Bangoura, K.; Traore, S. Evaluation of the Bacteriological Pollution of the Waters of the Lake of Sonfonia Commune of Ratoma (Republic of Guinea) 2021. *J. Agric. Chem. Environ.* **2023**, *12*, 142–151. [CrossRef]
45. Sidiki, S. Bauxite Mining in the Boké Region (Western Guinea): Method Used and Impacts on Physical Environment. *Eur. J. Sustain. Dev. Res.* **2019**, *3*, em0087. [CrossRef] [PubMed]
46. Knierzinger, J. The socio-political implications of bauxite mining in Guinea: A commodity chain perspective. *Extr. Ind. Soc.* **2014**, *1*, 20–27. [CrossRef]
47. Mamedov, V.I.; Makarova, M.A.; Korrea Gomesh, G.; Chausov, A.A.; Okonov, E.A.; Lopukhin, M.V. Bauxite-bearing lateritic covers of Sandaredi area, Republic of Guinea. *Int. Res. J.* **2016**, *49*, 114–135. [CrossRef]
48. Mamedov, V.I.; Chausov, A.A.; Okonov, E.A.; Makarova, M.A.; Boeva, N.M. The World's Largest Fouta Djallon–Mandingo Bauxite Province (West Africa): Part I. Background. *Geol. Ore Depos.* **2020**, *62*, 163–176. [CrossRef]
49. Abell, R.; Thieme, M.L.; Revenga, C.; Bryer, M.; Kottelat, M.; Bogutskaya, N.; Coad, B.; Mandrak, N.; Balderas, S.C.; Bussing, W.; et al. Freshwater Ecoregions of the World: A New Map of Biogeographic Units for Freshwater Biodiversity Conservation. *BioScience* **2008**, *58*, 403–414. [CrossRef]
50. *Ecosystem Profile: Guinean Forests of West Africa Biodiversity Hotspot*; Critical Ecosystem Partnership Fund; World Conservation Monitoring Centre: Cambridge, UK, 2015.
51. Budyko, M.I.; Lavrenko, E.M. *Sochava Physico-geographical Atlas of the World*; Academy of Sciences of the USSR and the Main Directorate of Geodesy and Cartography of the GGC of the USSR: Moscow, Russia, 1964; pp. 64–67, 130–131.
52. *Geology of the Republic of Guinea*; Geoprospects Ltd.; Lomonosov Moscow State University (Faculty of Geology): Russia, Moscow, 2011; Volume 1, pp. 10–17.
53. Jones, A.; Breuning-Madsen, H.; Brossard, M.; Dampha, A.; Dewitte, O.; Hallett, S.; Jones, R.; Kilasara, M.; Le Roux, P.; Micheli, E.; et al. *Soil Atlas of Africa*; EUR 25534 EN; Publications Office of the European Union: Luxembourg, 2013. [CrossRef]
54. Bolonin, A.V.; Mamedov, V.I.; Myznikov, I.K. Iron quartzites of the Simandou mountain (Republic of Guinea). *Ores Met.* **2022**, *3*, 57–77. [CrossRef]
55. Kuzin, S.V. Engineering-geological features of the lateritic weathering crust of Mesozoic dolerites in the central part of the Boke province in the Guinea republic. *Eng. Geol.* **2013**, *2*, 52–57.
56. European Space Agency. Sinergise. Copernicus Global Digital Elevation Model. Distributed by OpenTopography. 2021. Available online: https://portal.opentopography.org/datasetMetadata?otCollectionID=OT.032021.4326.1 (accessed on 13 April 2023).
57. Tabunshchik, V.; Gorbunov, R.; Gorbunova, T.; Pham, C.N.; Klyuchkina, A. Identification of river basins within northwestern slope of Crimean Mountains using various digital elevation models (ASTER GDEM, ALOS World 3D, Copernicus DEM, and SRTM DEM). *Front. Earth Sci.* **2023**, *11*, 1218823. [CrossRef]
58. Byamba, O.; Siberian State University of Geosystems and Technologies; Kasyanova, E.L. *Creation of River Network Model for Thematic Map Using GIS Technology*; Vestnik SSUGT (Siberian State University of Geosystems and Technologies): Novosibirsk, Russia, 2022; Volume 27, pp. 40–49. [CrossRef]
59. Ermolaev, O.P.; Mal'tsev, K.A.; Mukharamova, S.S.; Kharchenko, S.V.; Vedeneeva, E.A. Cartographic model of river basins of European Russia. *Geogr. Nat. Resour.* **2017**, *38*, 131–138. [CrossRef]
60. Copernicus Open Access Hub. Available online: https://scihub.copernicus.eu/dhus/#/home (accessed on 1 October 2023).
61. Tabunshchik, V.; Gorbunov, R.; Gorbunova, T. Anthropogenic Transformation of the River Basins of the Northwestern Slope of the Crimean Mountains (The Crimean Peninsula). *Land* **2022**, *11*, 2121. [CrossRef]
62. Earth Engine Data Catalog. Available online: https://developers.google.com/earth-engine/datasets (accessed on 1 October 2023).
63. Tabunschik, V.; Gorbunov, R.; Gorbunova, T. Unveiling Air Pollution in Crimean Mountain Rivers: Analysis of Sentinel-5 Satellite Images Using Google Earth Engine (GEE). *Remote Sens.* **2023**, *15*, 3364. [CrossRef]
64. Protected Areas. Available online: https://www.protectedplanet.net/country/GIN (accessed on 1 October 2023).
65. Hersbach, H.; Bell, B.; Berrisford, P.; Biavati, G.; Horányi, A.; Muñoz Sabater, J.; Nicolas, J.; Peubey, C.; Radu, R.; Rozum, I.; et al. ERA5 Hourly Data on Single Levels from 1940 to Present. Copernicus Climate Change Service (C3S) Climate Data Store (CDS). 2023. Available online: https://cds.climate.copernicus.eu/cdsapp#!/dataset/reanalysis-era5-single-levels?tab=overview (accessed on 1 October 2023).
66. Gharibvand, L.K.; Jamali, A.A.; Amiri, F. Changes in NO_2 and O_3 levels due to the pandemic lockdown in the industrial cities of Tehran and Arak, Iran using Sentinel 5P images, Google Earth Engine (GEE) and statistical analysis. *Stoch. Environ. Res. Risk Assess.* **2023**, *37*, 2023–2034. [CrossRef] [PubMed]

67. Kaplan, G.; Avdan, Z.Y.; Avdan, U. Spaceborne Nitrogen Dioxide Observations from the Sentinel-5P TROPOMI over Turkey. *Proceedings* **2019**, *18*, 4. [CrossRef]
68. Cakmak, N.; Yilmaz, O.S.; Sanli, F.B. Spatio-temporal Analysis of Pollutant Gases using Sentinel-5P TROPOMI Data on the Google Earth Engine during the COVID-19 Pandemic in the Marmara Region, Türkiye. *E-Zbornik* **2023**, *13*, 1–14. [CrossRef]
69. Nugroho, R.T. Analysis of The Effect of Large Population on Nitrogen Dioxide and Carbon Monoxide Levels in Java Island Using Sentinel-5P. *IOP Conf. Ser. Earth Environ. Sci.* **2023**, *1127*, 012028. [CrossRef]
70. Rehmat, R.; Rafique, L.; Irfan, M.; Ahmed, S.R.; Lahori, A.H.; Muhammadi, A.; Taha, M.; Vambol, S.; Shulga, M. Space-borne Air Quality Monitoring of Nitrogen dioxide (NO2) over Karachi and Lahore using Remote Sensing Tools. *Proc. Pak. Acad. Sci. B Life Environ. Sci.* **2023**, *60*, 3. [CrossRef]
71. Roman-Gonzalez, A.; Navarro-Raymundo, A.F.; Vargas-Cuentas, N.I. Air Pollution Monitoring in Peru Using Satellite Data During the Quarantine Due to COVID-19. *IEEE Aerosp. Electron. Syst. Mag.* **2020**, *35*, 73–79. [CrossRef]
72. Khasanah, U.K.; Nucifera, F. The Effect of the COVID-19 Pandemic on Nitrogen Dioxide (NO_2) Gas Concentration in Yogyakarta Special Province. In Proceedings of the 5th International Conference on Information and Communications Technology (ICOIACT), Yogyakarta, Indonesia, 24–25 August 2022; pp. 210–214. [CrossRef]
73. Jamei, E.; Jamei, Y.; Seyedmahmoudian, M.; Horan, B.; Mekhilef, S.; Stojcevski, A. Investigating the impacts of COVID-19 lockdown on air quality, surface Urban Heat Island, air temperature and lighting energy consumption in City of Melbourne. *Energy Strat. Rev.* **2022**, *44*, 100963. [CrossRef]
74. Morozova, A.; Sizov, O.; Elagin, P.; Lobzhanidze, N.; Fedash, A.; Mironova, M. Evaluation of the Impact of COVID-19 Restrictions on Air Pollution in Russia's Largest Cities. *Atmosphere* **2023**, *14*, 975. [CrossRef]
75. Sari, N.M.; Kuncoro, M.N.S. Monitoring Of CO, NO_2 And SO_2 Levels During The Covid-19 Pandemic In Iran Using Remote Sensing Imagery. *Geogr. Environ. Sustain.* **2021**, *14*, 183–191. [CrossRef]
76. Pandey, S.; van Nistelrooij, M.; Maasakkers, J.D.; Sutar, P.; Houweling, S.; Varon, D.J.; Tol, P.; Gains, D.; Worden, J.; Aben, I. Daily detection and quantification of methane leaks using Sentinel-3: A tiered satellite observation approach with Sentinel-2 and Sentinel-5p. *Remote Sens. Environ.* **2023**, *296*, 113716. [CrossRef]
77. Tariq, S.; Ul-Haq, Z.; Mariam, A.; Mehmood, U.; Ahmed, W. Assessment of air quality during worst wildfires in Mugla and Antalya regions of Turkey. *Nat. Hazards* **2022**, *115*, 1235–1254. [CrossRef]
78. Ihsan, Y.N.; Purba, N.P.; Faizal, I.; Anya, A.; Mulyani, P.G.; Anwar, S.K. Impact of the Pandemic COVID-19 to the Indonesia Seas. *Geoj. Tour. Geosites* **2022**, *40*, 30–36. [CrossRef]
79. Islam, Z.; Singh, S.K.; Ahirwar, S. Change In Nitrogen Dioxide (No2) Concentration Due To The Lockdown Amid The Covid-19 Pandemic In India. *Geogr. Environ. Sustain.* **2021**, *14*, 192–198. [CrossRef]
80. Dimitrova, M.; Trenchev, P. Space Distribution of NO2 Pollution over Bulgaria. *Aerosp. Res. Bulg.* **2023**, *35*, 28–33. [CrossRef]
81. Morozova, A.E.; Sizov, O.S.; Elagin, P.O.; Agzamov, N.A.; Fedash, A.V.; Lobzhanidze, N.E. Integral Assessment of Atmospheric Air Quality in the Largest Cities of Russia Based on TROPOMI (Sentinel-5P) Data for 2019–2020. *Cosm. Res.* **2022**, *60*, S57–S68. [CrossRef]
82. Wang, C.; Wang, T.; Wang, P.; Rakitin, V. Comparison and Validation of TROPOMI and OMI NO_2 Observations over China. *Atmosphere* **2020**, *11*, 636. [CrossRef]
83. Magro, C.; Nunes, L.; Gonçalves, O.C.; Neng, N.R.; Nogueira, J.M.F.; Rego, F.C.; Vieira, P. Atmospheric Trends of CO and CH_4 from Extreme Wildfires in Portugal Using Sentinel-5P TROPOMI Level-2 Data. *Fire* **2021**, *4*, 25. [CrossRef]
84. Safarianzengir, V.; Sobhani, B.; Yazdani, M.H.; Kianian, M. Monitoring, analysis and spatial and temporal zoning of air pollution (carbon monoxide) using Sentinel-5 satellite data for health management in Iran, located in the Middle East. *Air Qual. Atmos. Health* **2020**, *13*, 709–719. [CrossRef]
85. Yilmaz, O.S.; Acar, U.; Sanli, F.B.; Gulgen, F.; Ates, A.M. Mapping burn severity and monitoring CO content in Türkiye's 2021 Wildfires, using Sentinel-2 and Sentinel-5P satellite data on the GEE platform. *Earth Sci. Inform.* **2023**, *16*, 221–240. [CrossRef] [PubMed]